

Quarterly Report for
April - June 1999
Stanford Geothermal Program
DE-FG07-95ID13370

Table of Contents

1. MEASUREMENTS OF STEAM-WATER RELATIVE PERMEABILITY	1
1.1 BACKGROUND	1
1.2 EXPERIMENTS	4
1.3 FRACTURE FLOW EXPERIMENTS	10
1.4 DISCUSSION	11
1.5 CONCLUSIONS	11
2. AN EXPERIMENTAL INVESTIGATION OF BOILING HEAT CONVECTION WITH RADIAL FLOW IN A FRACTURE	13
2.1 INTRODUCTION	13
2.2 BOILING CONVECTION COEFFICIENT CALCULATION	13
2.3 REEVALUATION OF DATA AND VERIFICATION OF ACCURACY	15
2.4 FUTURE WORK	15
3. INFERRING ENDPOINT SATURATION FROM BOILING EXPERIMENTS AND FIELD MEASUREMENTS	17
3.1 INTRODUCTION	17
3.2 INFERRING ENDPOINT SATURATION FROM BOILING EXPERIMENTS	18
3.3 INFERRING ENDPOINT SATURATION FROM FIELD MEASUREMENTS	29
4. STEAM-WATER CAPILLARY PRESSURE	33
4.1 INTRODUCTION	33
4.2 THEORY	33
4.3 EXPERIMENTS	34
4.4 RESULTS	36
4.5 CONCLUSIONS	42
4.6 FUTURE WORK	43
5. ACCURATE MEASUREMENT OF STEAM FLOW PROPERTIES	45

5.1 SUMMARY	45
5.2 INTRODUCTION	45
5.3 EXPERIMENTS	45
5.4 RESULTS	49
5.5 DISCUSSION	52
5.6 CONCLUSIONS	53
5.7 FUTURE WORK	53
6. REFERENCES	55

1. MEASUREMENTS OF STEAM-WATER RELATIVE PERMEABILITY

This research project is currently being conducted by Research Assistant Glenn Mahiya and Professor Roland Horne. The aim of this project is to measure relative permeability relations for steam and water flowing simultaneously in rocks.

Reliable measurement of steam-water relative permeability functions is of great importance for geothermal reservoir performance simulation. Despite their importance, these functions are poorly known due to the lack of fundamental understanding of steam-water flows, and the difficulty of making direct measurements. The Stanford Geothermal Program has used an X-ray CT (Computer Tomography) scanner to obtain accurate saturation profiles by direct measurement. During the quarter, we have completed experiments with nitrogen-water flow and with steam-water flow and examined the effects of heat transfer and phase change by comparing these sets of results.

In porous rocks, it was found that the steam-water relative permeabilities follow Corey type relationships similar to those in nitrogen-water flow but that the irreducible gas phase saturation is smaller for steam than for nitrogen. The irreducible saturations represent substantial fractions of the recoverable energy in place yet are hard to determine in the field. Understanding the typical magnitude of irreducible saturations will lead to a much clearer forecast of geothermal field performance. In fracture flow, indirect measurements suggested that the relative permeabilities follow a linear (or "X-curve") behavior -- but there is still considerable uncertainty in the knowledge of this behavior.

1.1 BACKGROUND

The flow of steam and water through the interstices of geothermal rocks is governed by complex physical phenomena involving mechanical interaction between the two fluids, water and steam, as well as by the thermodynamic effects of boiling heat transfer. This complex interaction is commonly described in terms of the steam-water relative permeabilities, defined as a modification of Darcy's Law for single-phase flow:

$$q = \frac{k}{\mu} A \left(\frac{\Delta p}{L} \right) \quad (1.1)$$

where q , k , μ , A , L , Δp are volumetric fluid flow rate, absolute permeability, fluid viscosity, cross-sectional area, length and pressure drop over the length L , respectively. When steam and water flow simultaneously, each phase is governed by an independent flow equation:

$$k_i = k k_{ri} = \frac{q_i \mu_i L}{A \Delta p_i} \quad ; \quad i = \text{steam, water.} \quad (1.2)$$

Here k_i is effective permeability to phase i , q_i is volumetric fluid flow rate of phase i , and μ_i is viscosity of phase i . The nondimensional form of effective permeability, called the relative permeability (k_r), is defined as the ratio of effective permeability to absolute

permeability ($k_{ri}=k_i/k$). Relative permeabilities are generally expressed as a function of the wetting phase saturation (usually water in the case of steam-water flow).

Steam-water relative permeabilities have been shown to make a significant impact on the performance of geothermal reservoirs (Bodvarsson, O'Sullivan and Tsang, 1980), however in practice they are extremely difficult parameters to measure. For homogeneous porous media the commonly assumed relative permeabilities are the Corey expressions (Corey, 1954):

$$\begin{aligned} k_{rl} &= S^{*4} & (S^* < 1) \\ k_{rg} &= (1 - S^*)^2 (1 - S^{*2}) & (S^* < 1) \\ S^* &= (S - S_{lr}) / (S_{gr} - S_{lr}) \end{aligned} \quad (1.3)$$

where S_{gr} and S_{lr} are the irreducible or residual saturations for liquid and gas, respectively. For fractured media, it has been more common to assume that the relative permeabilities follow the linear relationships known as the "X-curves":

$$\begin{aligned} k_{rl} &= S^* & (S^* < 1) \\ k_{rg} &= (1 - S^*) & (S^* < 1) \\ S^* &= (S - S_{lr}) / (S_{gr} - S_{lr}) \end{aligned} \quad (1.4)$$

where it is common to assume the residual saturations S_{gr} and S_{lr} to be zero. These two types of relative permeability curve are illustrated in Figure 1.1.

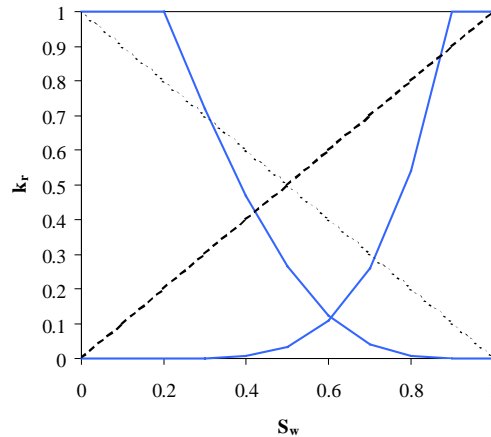


Figure 1.1: Corey (solid lines) and linear (dashed lines) relative permeability curves.

The principal problems in obtaining steam-water relative permeabilities experimentally are in measuring: (1) the in-place saturations, and (2) the flow rates of the two phases. In oil-water relative permeability experiments, the saturations and flow rates are determined easily by direct measurement of the inflows and outflows of the two phases, but in the case of steam and water the phases can easily change from one to the other, hence the difficulty. Table 1.1 summarizes 25 years of work in the determination of steam-water relative permeability, including the methods used to measure saturation. Despite the

number of independent studies, the results have proven to be inconsistent, hence confidence in the use of the results for commercial reservoir simulation has been low.

The Stanford Geothermal Program has conducted steam-water relative permeability experiments in two campaigns, one in the 1970s (Arihara, 1974, Chen et al., 1978, Council and Ramey, 1979) and more recently in the 1990s (Ambusso, 1996, Tovar, 1997, Satik, 1998, Mahiya, 1999). Since 1996, the Stanford measurements have used X-ray CT (Computer Tomography) methods to determine the in-place steam saturation. This powerful and accurate method allows for the steam-water distribution to be obtained at any place within the core (see Figure 1.2). Nonetheless, repeated studies still had difficulty in producing repeatable results that were consistent with earlier literature – the difficulty of determining the individual steam and water flow rates remained. One of our first successful measurements was by Ambusso (1996), Figure 1.3, who suggested that the steam-water relative permeabilities were best described by the X-curves. However, later measurements by Satik (1998), Figure 1.4, failed to confirm this and indicated that Corey type behavior was more likely (as had also been seen elsewhere for unconsolidated materials by Sanchez and Schechter, 1990).

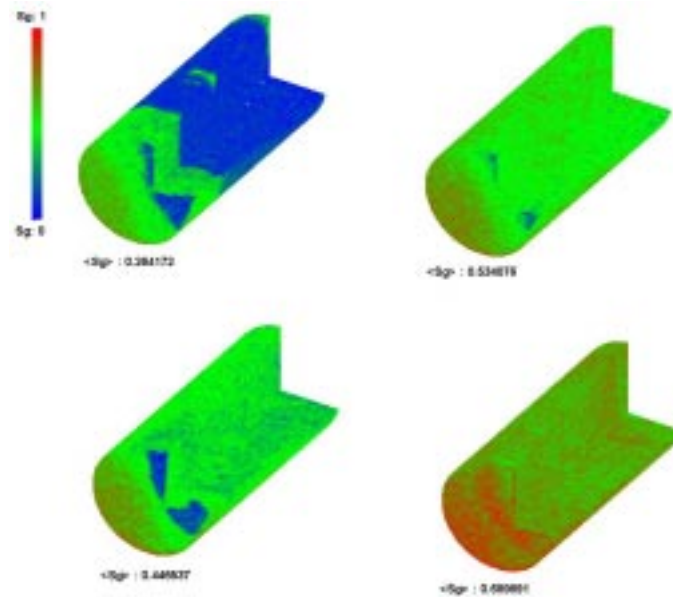


Figure 1.2: Steam distributions measured by X-ray CT, from Satik (1998).

The study by Sanchez and Schechter (1990) had used an adiabatic experiment, maintaining the heat in the sample by use of guard heaters. The experiments of Ambusso (1996) and Satik (1998) were nonadiabatic, mainly because ferrous heaters placed around the core would attenuate the X-rays and cause artifacts in the saturation measurement. In the nonadiabatic experiments, the phase flow rates were computed after carefully measuring the heat fluxes from the core; nonetheless, this computation increased the uncertainty of the results. Since the results of Satik (1998) differed from those of Ambusso (1996) (although similar to the results of Sanchez and Schechter, 1990) and were difficult to reproduce, in 1999 Mahiya undertook a new study, combining the adiabatic approach of Sanchez and Schechter (1990) with the X-ray CT measurement of saturation as used by Satik (1998). The study used a very thin film heater which avoided the problem of X-ray

attenuation. The measurements attained by Mahiya (1999) demonstrated repeatability of Satik's 1998 results, and were close to those of Sanchez and Schechter (1990). Thus it was finally possible to associate confidence to these measurements, and to conclude that steam-water relative permeability relationships are of the Corey type.

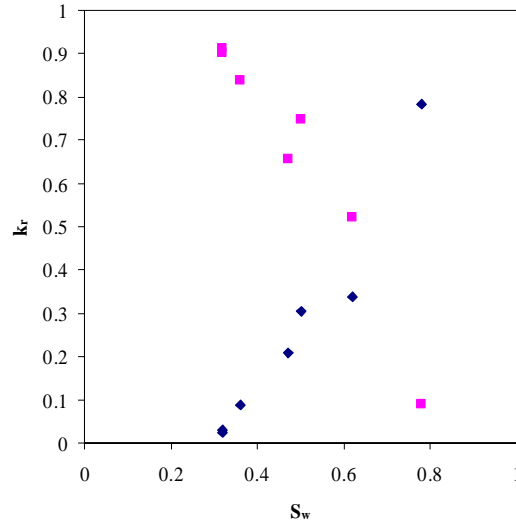


Figure 1.3: Experimental results from Ambusso (1996).

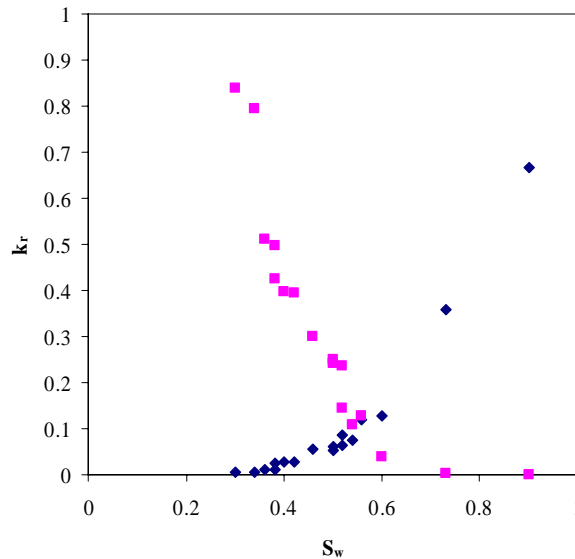


Figure 1.4: Experimental results from Satik (1998).

1.2 EXPERIMENTS

The physical parameters required to establish relative permeability curves are pressure, temperature, heat flux, flow rates and saturation. The experimental apparatus used by Satik (1998) and Mahiya (1999) made use of a nonmetallic coreholder made of the material PEEK, with a series of pressure and temperature measurements made along the interior axis of the core. Steam and water were injected independently into two separate ports at the inlet end of the coreholder, each with their own positive-displacement pump.

The water used for injection was deaerated by preboiling, and then reheated by immersion heaters that were constructed within the inlet endplate of the coreholder. This configuration reduced heat losses between the heater and the core entry that had been a concern to Sanchez and Schechter (1990). Heat losses from the core were cancelled out using thin-film guard heaters under automatic computer control.

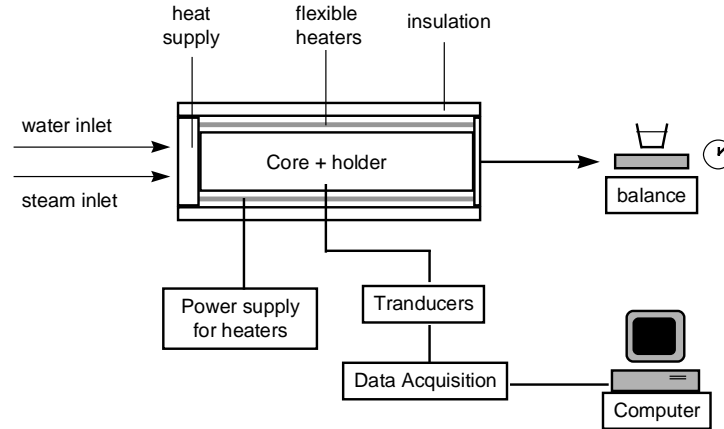


Figure 1.5: Experimental apparatus for the flow-through experiment using heat guards.

1.2.1 Experimental Configuration

Figure 1.5 shows a schematic of the apparatus that allowed real-time measurement of the required quantities. The experiment used a 43 cm Berea sandstone core with a nominal absolute permeability of 1200 md and a measured porosity of 24%. This was the same core used in experiments by Satik (1998). Pressures and temperatures were measured through ports at eight positions along the core spaced 5 cm apart. These ports connected the core to pressure transducers via plastic tubings, and provided tapping points into which thermocouple wires were inserted for temperature readings. A blanket of insulating fiber around this assembly partially reduced the escape of heat.

In order to achieve two-phase conditions in the core, dry steam and hot liquid water were injected separately into two ports at the inlet using two independent constant-displacement pumps. Injection rates were typically between 0 and 10 ml/min. Each stream of fluid used deionized water pumped from a common reservoir to a boiler and then to a condensing loop. This process eliminated dissolved air that would introduce errors in the saturation measurements. The deaerated water was then delivered to the heating head in the core inlet where each of the two streams was reheated to either steam or hot water. Steam and water then became mixed in the first few centimeters of the porous medium. Injection temperatures were typically of order 120°C, although the value varied somewhat from one step to the next. Fluid exited the core at atmospheric pressure and was directed to the sink where volumetric rate was checked using a graduated cylinder and timer, and compared with the injection rates specified at the two inlet pumps.

In-situ saturation values were determined from CT image arrays generated by the Picker Synerview 1200X X-ray CT scanner. The core assembly was mounted and secured on a stepper motor that allowed movement of the core in and out of the X-ray gantry with 1

cm interval. We were able to take measurements at 41 sections along the core. Figure 1.6 shows the major components of the experimental apparatus and the CT scanner.

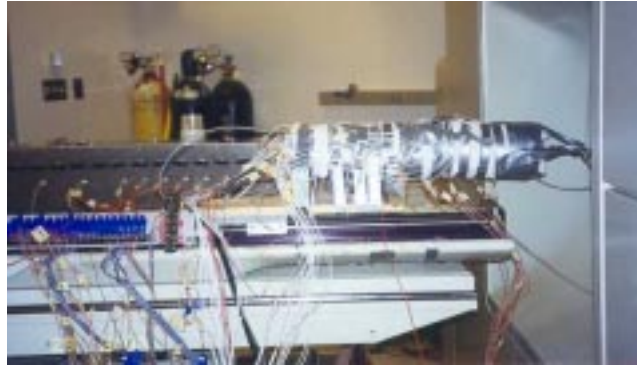


Figure 1.6: Core assembly mounted on stepper motor drive in the X-ray CT scanner.

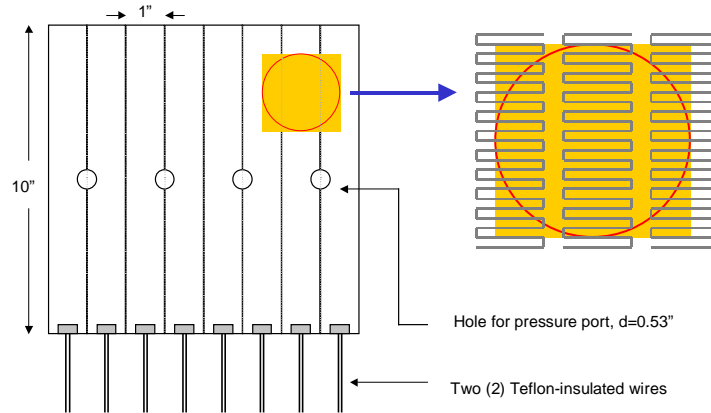


Figure 1.7: Schematic of flexible heaters.

1.2.2 Flexible Guard Heaters

Despite the thick layer of insulation around the coreholder, there was still considerable heat escaping from the core in Satik's 1998 experiments. In the new experiment, the exact amount of heat that was lost was supplied back to the system, so that overall heat loss would be negligible, if not zero. We designed flexible heaters custom-made for this purpose. Figure 1.7 shows a schematic of one of the Kapton-insulated flexible heaters.

Since single-sheet heaters long enough to completely cover the core were not available, we used two separate 20×25 cm and 23×25 cm sheets. Holes with 1.34 cm diameters were provided to allow for the protruding pressure ports along the core length. Each sheet was an array of eight or nine 2.5×25 cm strips of heating elements that could be controlled independently. In effect, we had 17 different heaters, each rated at 0.4 W/cm² at 115 volts. Since the heaters required only a small amount of current to operate, we used a transformer to step-down the voltage from 120 VAC to 60 VAC. The flexible thin-film heaters did not cause significant X-ray interference.

Each of the 17 independent heating strips was controlled in response to its own heat flux sensor placed under the heater on the surface of the coreholder. The voltage to the heater strip was switched on and off with an on-time sufficient to supply enough heat to balance the energy being lost from the core. In most cases the switching cycle was 20-30 times a minute. Each strip was controlled independently, using a 32-channel National Instruments SCXI 1163-R solid-state relay output module.

1.2.3 Experimental Process

The core preparation procedure involved drying the core by subjecting it to 120°C in an oven and simultaneously pulling a vacuum. The core had previously been baked at higher temperatures for the purpose of deactivating clays in the rock. Once dried, the core was assembled into the coreholder and bonded in place using epoxy. A dry X-ray scan was then made to obtain the CT attenuation values CT_{dry} . The core was then fully saturated with water and scanned to obtain the values of CT_{wet} , and from these the porosity distribution was obtained. The next step was to flow hot liquid water to obtain CT_{hw} which was necessary for calculating experimental saturations. The completion of this scan marked the start of the actual flow-through experiments. The electrical power was increased in stages by changing the voltage settings of the two heaters that generated dry steam and hot water. During this staged procedure the wetting phase (water) was displaced by the nonwetting phase (steam) and hence the flow was a drainage process. At each stage, two-phase flow in the core was allowed to stabilize before an X-ray scan was performed. At every stabilization, pressure, temperature and heat fluxes from the core were measured. The maximum steam saturation was reached by injecting only steam at the inlet. Once maximum steam saturation was achieved, input power to the steam and water heaters was gradually decreased to create an imbibition process whereby liquid water displaced steam. The values of relative permeability to steam and water were then computed after choosing sections of the core in which the saturation could be seen (in the CT scans) to be constant. One important aspect of the computation was the requirement to correct for the Klinkenberg slip effect, as described by Li and Horne (1999).

1.2.4 Results

The results of the 1999 experiments by Mahiya are shown in Figure 1.8. The behavior of the relative permeability curves in these measurements is clearly of the Corey type, and shows little difference between drainage and imbibition processes. The relative permeability values are in close agreement with the values of both Satik (1998), for the same rock, and with the values of Sanchez and Schechter (1990), for an unconsolidated sand. Figure 1.9 shows the comparison in terms of k_{rs} vs. k_{rw} , showing the agreement between these three measurements, and the substantial difference of the results of Ambusso (1996). Also shown on Figure 1.9 are the relative permeability values for nitrogen and water (imbibition process), as measured by Li and Nassori in the same core and experimental apparatus used by Mahiya (1999) – although similar in shape, it is clear that the relative permeability to nitrogen is less than that to steam, mainly because the irreducible nitrogen saturation (about 0.3) is significantly greater than the irreducible steam saturation (about 0.2). The same data, plotted as a function of water saturation in

Figure 1.10, shows that it is the gas relative permeability that differs most prominently between steam and nitrogen -- the water relative permeabilities are almost the same.

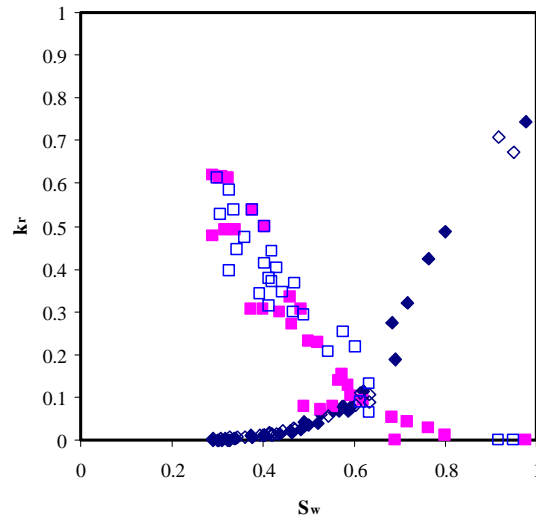


Figure 1.8: Experimental results from Mahiya (1999) adiabatic experiment. Closed symbols, drainage curves; open symbols, imbibition curves.

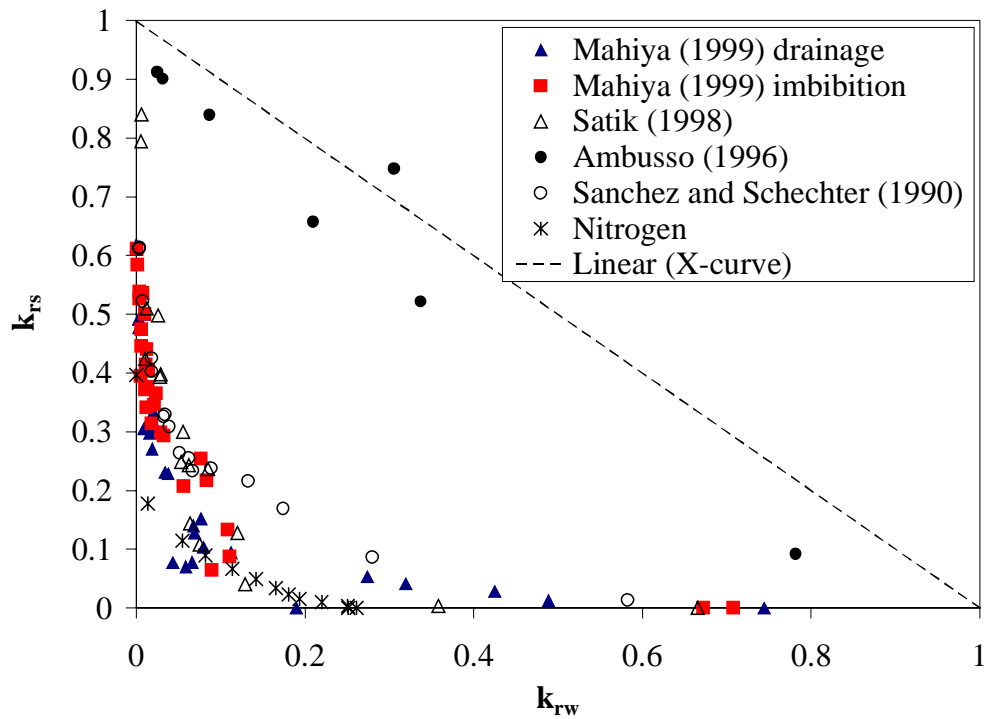


Figure 1.9: Comparison of results, k_{rs} vs. k_{rw} .

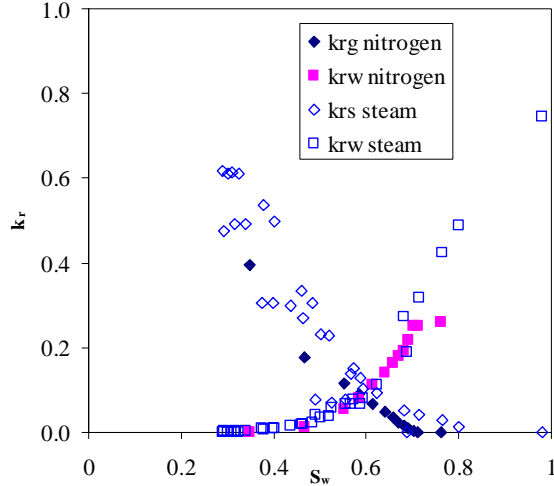


Figure 1.10: Comparison between steam-water (open symbols) and nitrogen-water imbibition (closed symbols) relative permeabilities on the same rock core.

Although we may call the results of the experiments of "Corey type", in fact the values of the relative permeabilities are better fit to the more general relations, of the type suggested by Honarpour et al. (1982):

$$k_{rs} = k_{rs0} \frac{(1 - S_w - S_{sr})^{n_s}}{(1 - S_{wr} - S_{sr})} \quad (1.5)$$

$$k_{rw} = k_{rw0} \frac{(S_w - S_{wr})^{n_w}}{(1 - S_{wr} - S_{sr})}$$

where S_{wr} and S_{sr} are the water and steam irreducible saturations respectively. Figure 1.11 shows a match to the data from the combined drainage and imbibition results of Mahiya (1999). The values of the best fit parameters are $k_{rs0} = 0.63$, $k_{rw0} = 0.49$, $S_{sr} = 0.13$, $S_{wr} = 0.27$, $n_s = 2.04$ and $n_w = 2.65$. The value of n_s (2.04) is very close to the Corey value of 2 from Eq. (1.3), while the value of n_w (2.65) is less than the Corey value of 4.

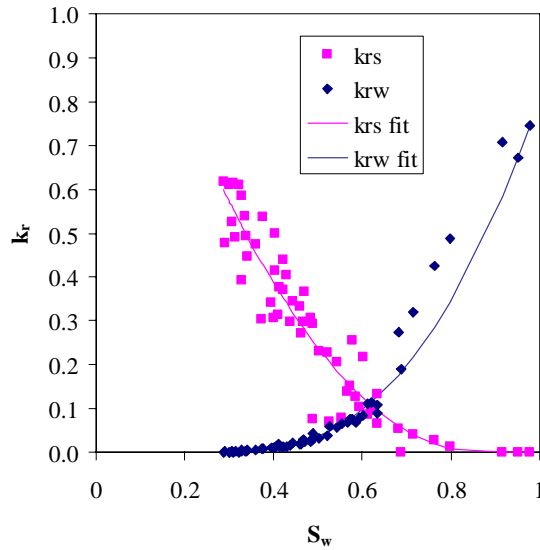


Figure 1.11: Fit to Mahiya (1999) results.

1.3 FRACTURE FLOW EXPERIMENTS

The relative permeabilities resulting from multiphase flow in fractures have received considerably less attention in published literature than those in porous media. The classically assumed X-curves (Figure 1.1) originated from experiments by Romm (1966) using oil-water flow in smooth fractures divided into strips in the flow direction. In Romm's experiments, the limiting values of the relative permeabilities k_{ro0} and k_{rw0} were both 1.0, and the residual saturations were both 0.0. That is, the sum of the relative permeabilities would always be one. More recent oil-water experiments in smooth fractures by Pan et al. (1996) also showed the residual saturations to be both 0.0, but the limiting k_{ro0} and k_{rw0} values were less than 1.0. Similar results were inferred in air-water flow in rough-walled fractures by Rangel-German et al. (1999).

Other experiments in rough-walled fractures have shown different kinds of relative permeability behavior. Fourar et al. (1993) conducted air-water experiments in both smooth- and rough-walled fractures, and proposed that the relative permeability concept was not useful to describe multiphase flow in fractures since the apparent relative permeability values would be functions of velocity. Even so, the apparent relative permeability curves shown in Fourar et al. (1993) do not appear to follow either X-curve or Corey behavior at any velocity. Persoff and Pruess (1995) measured air-water relative permeabilities in rough-walled fractures, and also concluded that the values differ from either Corey or linear behavior (showing lower values than either of those two models).

The theoretical study by Pruess and Tsang (1990) suggested that relative permeabilities in fractures may add up to considerably less than one, although the theory specifically excludes the possibility of "blobs" of one phase being conveyed by the other. The study also predicted ranges of saturation values at which neither phase can flow at all. Rossen and Kumar (1992), in another study that released the "blob transport" exclusion, advanced a theory that suggests a range of possibilities between the "sub-Corey" results of Pruess and Tsang (1990) at the lower end and the X-curves at the upper end.

All of the experimental studies mentioned so far in this section have been for air-water or oil-water flow. However, in fractures steam-water flow experiments have proven to be much more difficult, for the same reasons described in Section 1 for porous media. In one study, Wang and Horne (1999) inferred the steam-water relative permeabilities indirectly from experiments in a rough-walled fracture constructed of two plates of shower glass. 100°C water and steam flowed radially inward through the fracture towards a central port at which a vacuum was applied. Matching the observed temperature distribution in the fracture revealed that the observations could be replicated using a numerical simulation only if the relative permeability model was of the X-curve type (Figure 1.12).

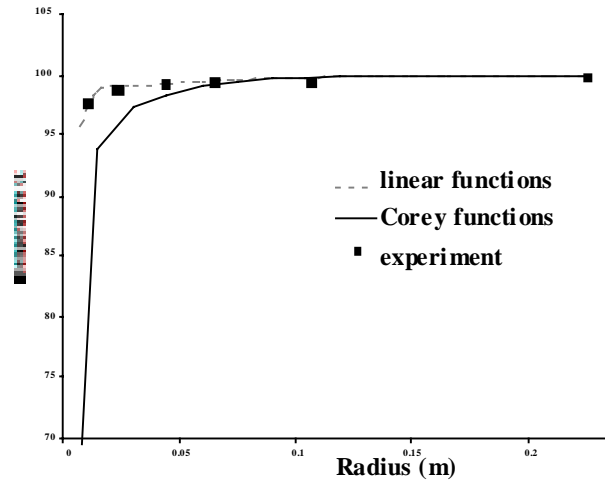


Figure 1.12: Fracture flow (temperature vs. radius) results from Wang and Horne (1999). Match using X-curves shown as dashed line, match using Corey curves shown as solid line.

1.4 DISCUSSION

The combined results of Satik (1998) and Mahiya (1999) established repeatability of the relative permeability measurements, and confirmed that these parameters follow the Corey type of behavior for flow in a porous rock. The similarity to the measurements of Sanchez and Schechter (1990) in unconsolidated sand adds further credence to this observation.

An important question to be raised is why the results of Ambusso (1996) were so different. The prominent deviation found by Satik (1998) provided significant confusion as to which of the two styles of relative permeability curve is the more appropriate. The confirming measurements by Mahiya (1999) suggest that it is the Corey type of behavior that is correct. It could be concluded that the rock in the Ambusso (1996) experiment had cracked, perhaps at the epoxy confinement, or maybe that the less sophisticated method of determining steam and water flow rates resulted in greater experimental error.

1.5 CONCLUSIONS

1. Steam-water relative permeabilities in a porous rock have been shown to follow Corey-type behavior.
2. This behavior has been confirmed in repeated experiments, and by comparison with earlier published results.
3. Proper interpretation of steam-water experiments at close to atmospheric pressure must include the influence of Klinkenberg slip effect.
4. Steam-water flow is similar to nitrogen water flow, except that the relative permeability to steam is greater than that to nitrogen, and the irreducible nitrogen saturation is greater than the irreducible steam saturation.
5. Steam-water relative permeabilities for flow in fractures are still unknown. Some steam-water and oil-water fracture flow experiments imply X-curve (linear) type of

behavior, however other experiments using air and water imply even lower phase mobility than would be implied by Corey type behavior.

In a real geothermal rock, steam and water will flow simultaneously in both fractures and in the porous matrix. The combination of these two flow processes may result in an effective relative permeability behavior that differs from either the Corey-type or the X-curve type of flow. The effect of this combination of behaviors has yet to be determined.

Table 1.1: Previous experiments relevant to steam-water relative permeabilities.

Reference	Year	Experiment type	Saturation technique	Core type
Mahiya	1999	Steam-water	CT scanner	Berea sandstone
Satik	1998	Steam-water	CT scanner	Berea sandstone
Ambusso	1996	Steam-water	CT scanner	Berea sandstone
Piquemal	1994	Steam-water	Gamma ray	Unconsolidated sand
Closmann and Vinegar	1988	Steam-water-oil	CT scanner	Natural core
Sanchez and Schechter	1987	Steam-water	Tracer	Unconsolidated sand
Verma and Pruess	1986	Steam-water	Gamma ray	Unconsolidated sand
Monsalve et al.	1984	Surfactant-steam-water	Tracer	Berea sandstone
Counsil and Ramey	1979	Steam-water	Capacitance probe	Consolidated synthetic
Horne and Ramey	1978	Steam-water	Production history	Field study
Chen et al.	1978	Steam-water	Capacitance probe	Consolidated synthetic
Grant	1977	Steam-water	Production history	Field study
Trimble and Menzie	1975	Steam-water-oil	Did not measure	Berea sandstone
Arihara	1974	Steam-water	Did not measure	Consolidated core

2. AN EXPERIMENTAL INVESTIGATION OF BOILING HEAT CONVECTION WITH RADIAL FLOW IN A FRACTURE

This project is being conducted by Research Assistant Robb Barnitt and Professor Roland Horne. The goal is to investigate and compare the heat flux and temperature gradients that develop during boiling within fractures. This project intends to develop a boiling convection coefficient for use in calculating heat transfer with boiling in fractured geothermal rock. Improved understanding and modeling of heat transfer in a fracture will ultimately lead to better strategies for injection into fractured geothermal reservoirs.

2.1 INTRODUCTION

Work conducted this quarter focussed upon evaluation of data from the experiment conducted in January 1999. This experiment sought to investigate and compare the heat flux and temperature gradients that develop during boiling with liquid injection into a radial fracture, and examine the differences in behavior dependant upon the nature of the fracture boundary matrix. The experiments were designed to quantify the heat flux associated with liquid water flashing to steam in a fracture, and to investigate the degree of coupling between the heat flux and the vapor fraction flowing in the fracture. The data was used in the calculation of boiling heat transfer coefficients at varying injection rates for the two experimental materials: aluminum and sandstone. Other methods of calculation of these boiling heat transfer coefficients, or boiling convection coefficients, were employed to verify the accuracy of the experimental apparatus and method.

2.2 BOILING CONVECTION COEFFICIENT CALCULATION

The boiling convection coefficient is defined as:

$$h_c = q / \Delta T_e \quad (2.1)$$

where q is the measured heat flux (W/m^2), and ΔT_e ($^{\circ}\text{K}$) is the excess temperature required for the onset of nucleate boiling. ΔT_e is defined as the difference between the temperature of the surface (T_{surf}) upon which boiling occurs, and the saturated temperature of the boiling liquid (T_{sat}). The boiling convection coefficient h_c has units $\text{W}/\text{m}^2\text{-K}$.

Aluminum Disk

During the course of the experiment, temperature data was collected once steady-state conditions were achieved at each of three injection rates. The temperature gradient observed across the central axis of the disk was applied to Fourier's Law to obtain a heat flux q . This temperature gradient was extrapolated across the fracture surface (top of disk) to gain the value of T_{surf} . Thermocouples oriented within the fracture aperture during the experiment provided the value of T_{sat} .

These values were obtained for each of the three injection rates, 15, 30, and 60 ml/min. However, the data collected during the 60 ml/min injection phase were flawed such that these calculations could not be applied. The extrapolated value of T_{surf} was lower than

that of T_{sat} . This produced an excess temperature value less than zero, which is impossible. Due to the orientation of the thermocouples recording temperature gradients within the aluminum disk 1.5 cm from the disk center, it is believed that conductive cooling from the cooler water injected at the disk center caused a radial temperature gradient that was not recorded and cannot be accounted for using the calculation above. Therefore, the data collected during the 60 ml/min injection rate phase of the experiment cannot be evaluated as valid data. Table 2.1 presents the measured ΔT_e , and calculated q and h_c for the two remaining injection rates.

Table 2.1: Comparison of boiling convection coefficients with varying injection rate for aluminum.

Injection Rate	15 ml/min	30 ml/min
Heat Flux q (W/m ²)	27436.62	28469.64
Excess Temperature ΔT_e (K)	1.339106	0.465308
Boiling Convection Coefficient h_c (W/m ² -K)	20488.76	61184.55

Sandstone Disk

As with the temperature data collected during the aluminum disk experiment, calculations were based upon temperatures averaged across thermocouples once steady-state had been achieved. The temperature gradient observed across the central axis of the disk was applied to Fourier's Law to obtain a heat flux q . However, due to the presence of boiling at a certain depth below the surface of the fracture (top of disk), the temperature gradient was markedly different between the middle and top of the porous sandstone. Therefore, the gradient closest to the fracture surface was extrapolated to determine T_{surf} . Thermocouples oriented within the fracture aperture during the experiment provided the value of T_{sat} . Table 2.2 presents the calculated values for each of the three injection rates.

Table 2.2: Comparison of boiling convection coefficients with varying injection rate for sandstone.

Injection Rate	15 ml/min	30 ml/min	60 ml/min
Heat Flux q (W/m ²)	34775.18	31434.97	22918.37
Excess Temperature ΔT_e (K)	1.208922	3.261846	4.0698
Boiling Convection Coefficient h_c (W/m ² -K)	28765.46	9637.17	5631.33

It is interesting to note that with increasing injection rate, the heat flux increased in the case of aluminum, but decreased in the case of the sandstone. Additionally, the boiling convection coefficient increased with increasing injection rate for aluminum, but decreased for sandstone. Although there are currently only two data points for aluminum, these trends are presented in Figure 2.1.

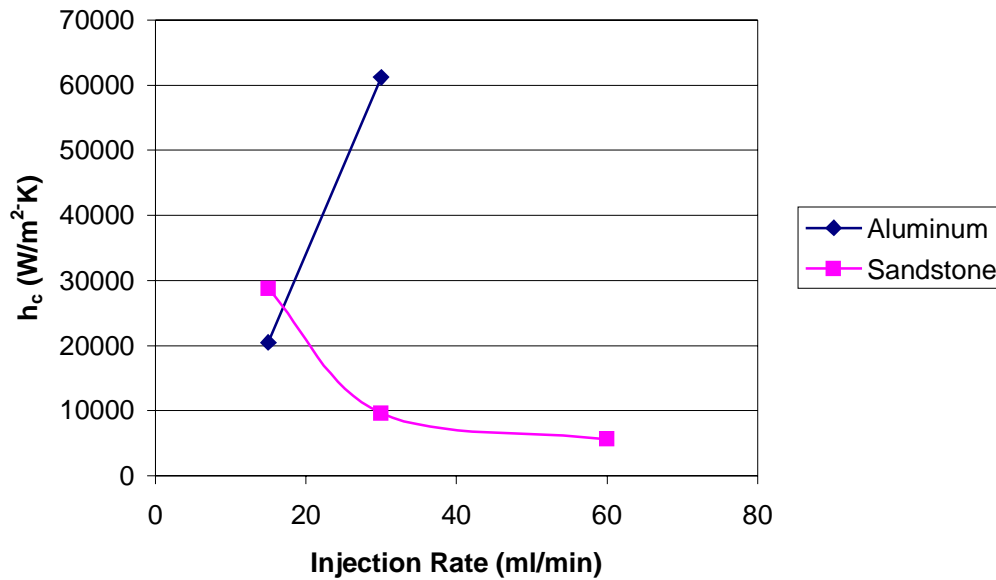


Figure 2.1: Boiling convection coefficient comparison.

2.3 REEVALUATION OF DATA AND VERIFICATION OF ACCURACY

An additional benefit of including the nonporous aluminum in the experiment is the ability to compare calculated values that describe the boiling process to known values using established equations. Comparison of the experimental versus previously known serves to provide assurance that the experimental apparatus furnishes accurate data.

Experimental data collected during the 15 ml/min injection rate aluminum phase was used for a rough approximation of h_c using the dimensionless Nusselt, Jakob, and Prandtl numbers, as well as an experimental constant. This check on data and calculations is merely an approximation because the experimental constant employed applies to brass, not aluminum. However, the calculated h_c was slightly less than one order of magnitude below the h_c calculated using the procedure described in Section 2.2.

2.4 FUTURE WORK

The previously executed experiment using the aluminum disk will be redone. This will provide additional data points to observe the behavior of heat flux and boiling convection coefficient variance with injection rate. An improvement upon the previous experimental apparatus will be the installation of 12.5 micron diameter thermocouples cemented to the surface upon which boiling occurs. This will eliminate the need to extrapolate the value of T_{surf} from a certain temperature gradient within the disk. If successful, these thermocouples will also be employed in the future graywacke disk experiment.

Another length of Geysers core has been obtained for use in rerunning the experiment with a graywacke disk prepared similarly to the sandstone and aluminum disks. The new graywacke disk will be prepared using a surface grinder, and drilled to specifications. Figure 2.2 illustrates the planned orientation of drilled holes to accommodate thermocouples with an exact fit.

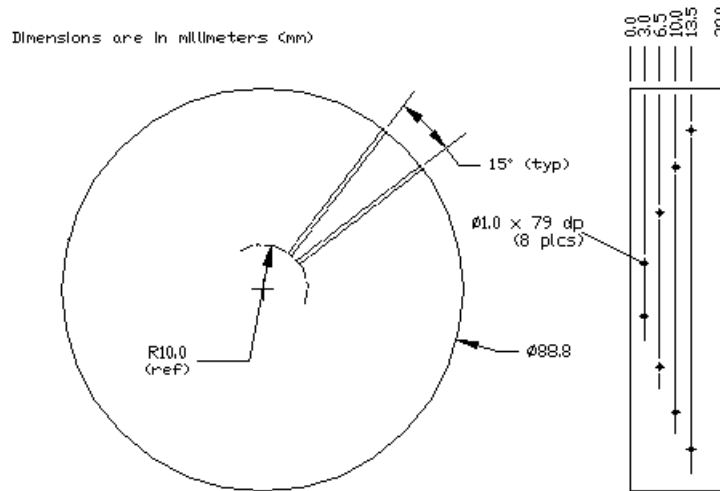


Figure 2.2: Thermocouple placement for graywacke disk in future experiment.

The heat flux sensors installed for this experiment will be checked and calibrated, as will the data acquisition system. This should eliminate the problems experienced in the previous experiments which involved heat flux sensor malfunction and incomplete data. The experiment will then be rerun using the same experimental procedure as before.

Previous experimental results indicated that low porosity, low permeability Geysers graywacke behaves unlike the sandstone or aluminum. The temperature gradient indicated that vaporization occurred beneath the fracture surface, isolating the boiling in the pores from the flow conditions in the fracture. Although this general behavior is expected, the new experiment will refine the accuracy of measuring the temperature gradients. Additionally, a clearer relationship between observed behavior and collected data will be available for comparison between all three experimental materials.

3. INFERRING ENDPOINT SATURATION FROM BOILING EXPERIMENTS AND FIELD MEASUREMENTS

This project is being conducted by Research Assistant Rodolfo Belen Jr. and Prof. Roland Horne. The aim is to determine the endpoint saturation of steam and liquid water relative permeability curves of geothermal reservoir rocks.

3.1 INTRODUCTION

Relative permeability is important in describing the flow of two-phase steam in geothermal reservoirs. Presently, however, relative permeability relations for steam and liquid water are not completely understood. Permeability relations are normally adopted from field data or from nitrogen and water flow experiments.

The experimental determination of steam and liquid water relative permeabilities is a central target of the Stanford Geothermal Program. Flow-through experiments on Berea sandstones were performed by Ambusso (1996), Satik (1998) and Mahiya (1999) that made use of X-ray computer tomography to determine steam saturation profiles. In a different approach, numerical simulation was used by Guerrero et al. (1998) to infer relative permeabilities of Berea sandstones, based on temperature, pressure, and steam saturation data obtained from steady state boiling experiments performed by Satik (1997).

All of these earlier studies used Berea sandstone in order to capitalize on its larger permeability relative to geothermal rocks, which enabled the experiments to be performed in reasonable time. This study aims to extend the understanding to low permeability geothermal rocks by determining only the endpoint saturations of the relative permeability curves. The endpoint or irreducible or immobile saturation of a certain phase is the saturation at which that phase becomes mobile in multiphase flow.

Combining information about the endpoint saturations from the “slow” geothermal rock experiments with information about the general shape of the relative permeability curves from the “faster” sandstone rock experiments will completely define the steam-liquid water relative permeability behavior.

Furthermore, determination of the irreducible water saturation will provide a better understanding of the adsorption characteristics and fluid storage capacities of geothermal rocks. This will be valuable in accurately estimating the size of the available resource in vapor-dominated reservoirs as well as liquid-dominated reservoirs that are experiencing dry out due to exploitation.

The objective of this study is to determine the endpoint saturation of the steam and liquid water relative permeability curves of geothermal rocks by inference from pressure, temperature and saturation data obtained from boiling experiments as well as inference from field measurements of temperature and flowing enthalpy.

3.2 INFERRING ENDPOINT SATURATION FROM BOILING EXPERIMENTS

Results of previous steady state boiling experiments performed by Satik (1997) were analyzed to investigate whether endpoint saturations can be inferred from the experimental data obtained.

3.2.1 Experimental Design of Boiling Experiments

In 1996 and 1997, Satik performed a series of boiling experiments using Berea sandstone cores. The objective of the study was to further the understanding of the boiling process in porous media and to ultimately obtain capillary functions and relative permeability relations for steam and liquid water. The steady state boiling experiments involved the heating of a rock saturated with liquid water and observing the boiling process by continuous measurement of pressure, temperature, heat flux and steam saturation within the rock. The X-ray CT scanner was used to visualize the boiling process and to determine the three-dimensional fluid distributions within the rock.

These experiments are analogous to drainage experiments in oil and water systems, in which oil, the non-wetting fluid, is injected into a rock saturated with water, the wetting fluid, to displace the water from the rock. However, in the case of the boiling experiments, steam produced by heating the water-saturated rock displaces the liquid water from the rock.

The experimental set-up consisted of a core holder housing the Berea sandstone core, a data acquisition system, a vacuum pump, a water pump and a balance (Figure 3.1).

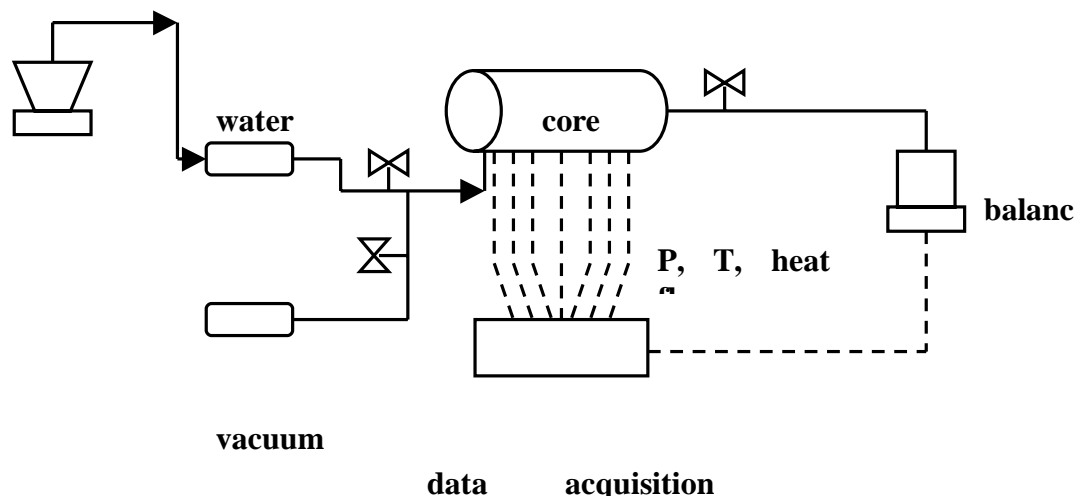


Figure 3.1: Configuration of boiling experiments.

The core was insulated with a fiber blanket to minimize heat losses. The heater was attached to one end of the core that was closed to fluid flow. The other end was connected to a water reservoir placed on a balance that was used to monitor the amount of water displaced from the core during the boiling process. Pressure, temperature and heat flux were measured in the core using pressure transducers, thermocouples and heat flux sensors respectively and were automatically recorded in a data acquisition system.

The core was first dried and then vacuumed to remove air inside the pore spaces. The core was then scanned at every 1-cm increment to obtain dry-core CT values that will be used in computing for the steam saturations. The core was then saturated with deaerated water and then scanned again at the same locations to obtain wet-core CT values. The heater was then turned on and pressure, temperature and heat flux were continuously measured during each heating step until steady state conditions were reached. Steady state was reached when no more water flows out of the core and when pressure, temperature and heat flux measurements had stabilized. At the same time, the core was scanned again to obtain CT values that were used to calculate the steam saturation distribution. The heating rate was increased and the procedure was repeated. Several experiments were performed in which the core was mounted vertically and horizontally.

3.2.2 Results of Boiling Experiments

It was observed that as the heating rate was increased, the steady state steam saturation data indicated a progressive boiling process with the formation of distinct regions of steam, two-phase and liquid water. Figures 3.2 to 3.4 are the steam saturation, pressure and temperature profiles of a bottom-heating vertical boiling experiment performed by Satik (1997) showing the formation of two-phase and liquid regions within the core as the boiling experiment progressed. The sudden drop in the steam saturation near the heater end of the core that marks the transition from steam to two-phase conditions is designated here as the elbow in the saturation profile.

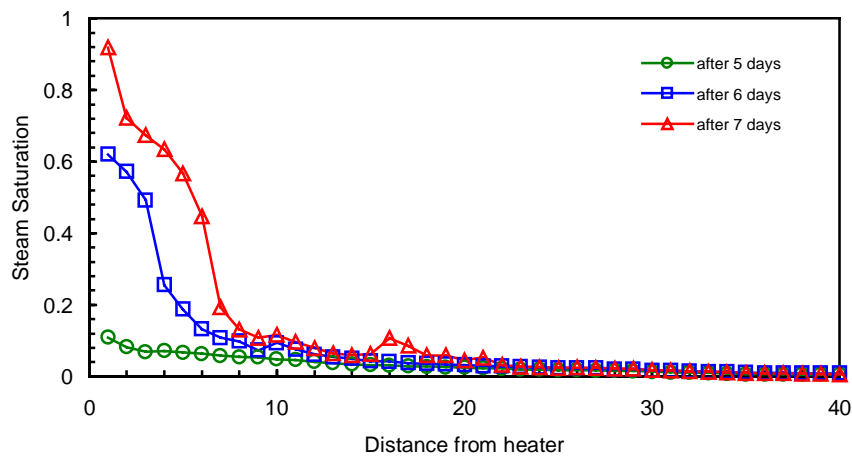


Figure 3.2: Steam saturation profile with time and distance from heater (Satik 1997).

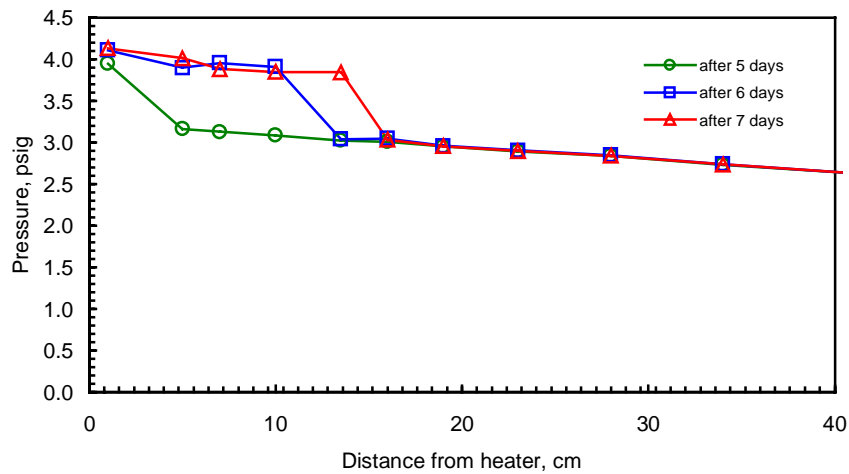


Figure 3.3: Pressure profile with time and distance from heater (Satik 1997).

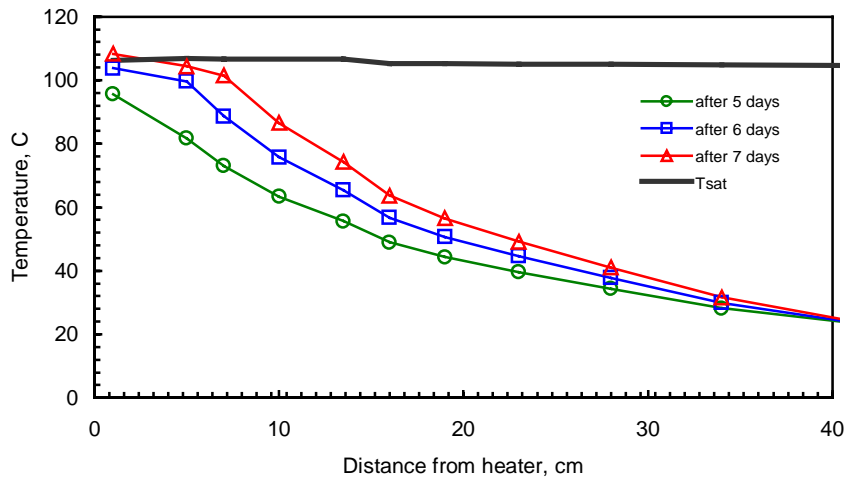


Figure 3.4: Temperature profile with time and distance from heater (Satik 1997).

3.2.3 Sensitivity Analysis of Boiling Experiments

It is hypothesized that the irreducible water saturation can be inferred from the elbow in the steam saturation profile. Analyzing the sensitivity of the boiling process to the irreducible water saturation through numerical modeling will test the validity of the hypothesis. The boiling process was simulated using different values of the endpoint water saturation of the relative permeability curves. The pressure, temperature and saturation profiles were predicted to verify if the elbow in the saturation profiles could be correlated with the irreducible water saturation.

In 1998, Guerrero et al. developed a two-dimensional radial iTOUGH2 model to infer relative permeability relations from the results of the boiling experiments. The same model

was used in the sensitivity analysis but the grids were refined to give a better resolution of the variations in the steam saturation near the heater end of the core.

Forward calculations in iTOUGH2 were performed to predict the pressure, temperature, and steam saturation profiles along the core. It is assumed that linear steam-liquid water relative permeability functions and Leverett capillary functions govern the flow of two-phase steam in the sandstone core.

The non-adiabatic boiling process was simulated using constant and variable heating rates. Figures 3.5 to 3.10 show the steam saturation and temperature profiles with time and with distance from the heater end for constant heating rates of 1, 2, 3 and 3.5 Watts. The endpoint water saturation of the linear relative permeability curves used in the simulation was assumed to be equal to 0.2 in all four cases. Steam saturation and temperature at the center of the core were plotted up to a distance 5 cm away from the heater end at different times.

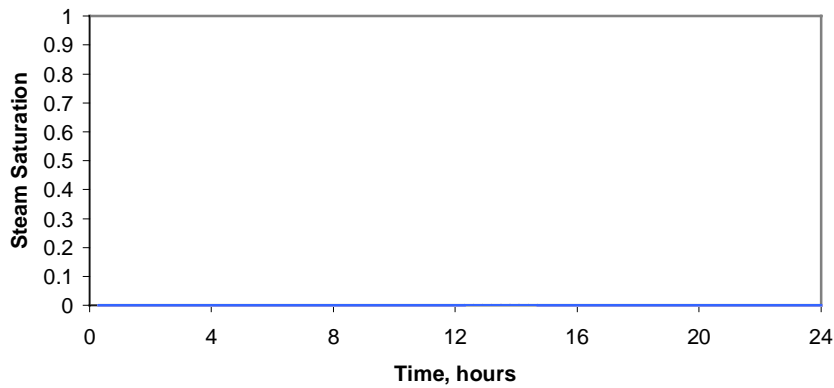


Figure 3.5a: Steam saturation profile at a constant heating rate = 1 W.

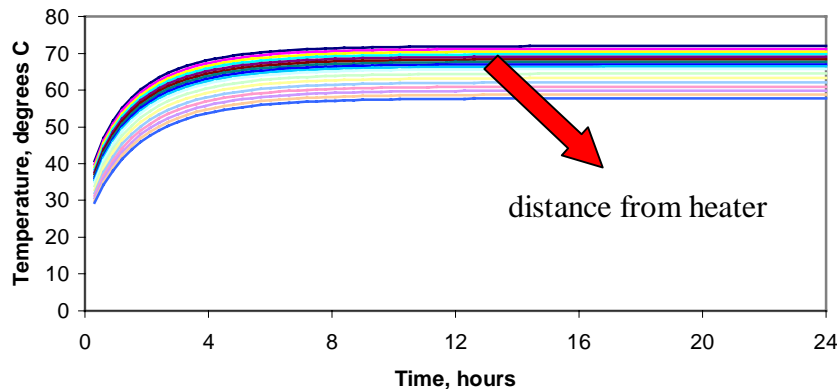


Figure 3.5b: Temperature profile at a constant heating rate = 1 W.

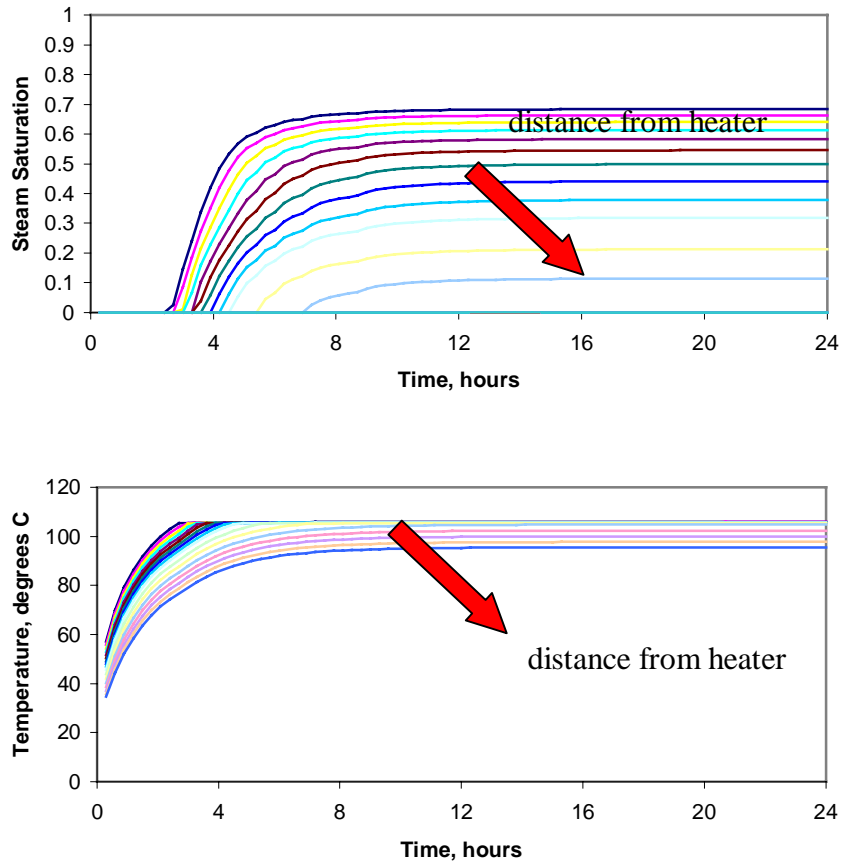


Figure 3.6: Steam saturation and temperature profiles at a constant heating rate = 2 W.

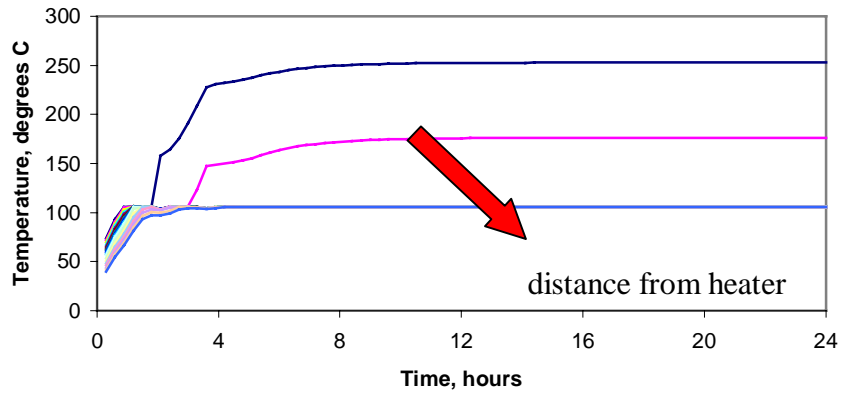
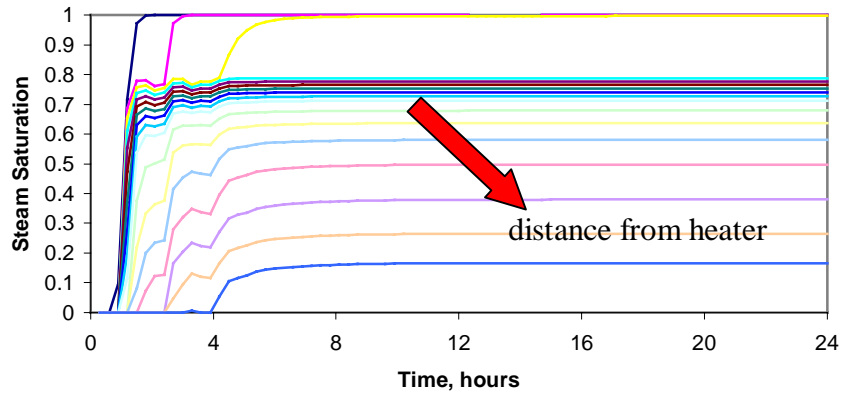


Figure 3.7: Steam saturation and temperature profiles at a constant heating rate = 3 W.

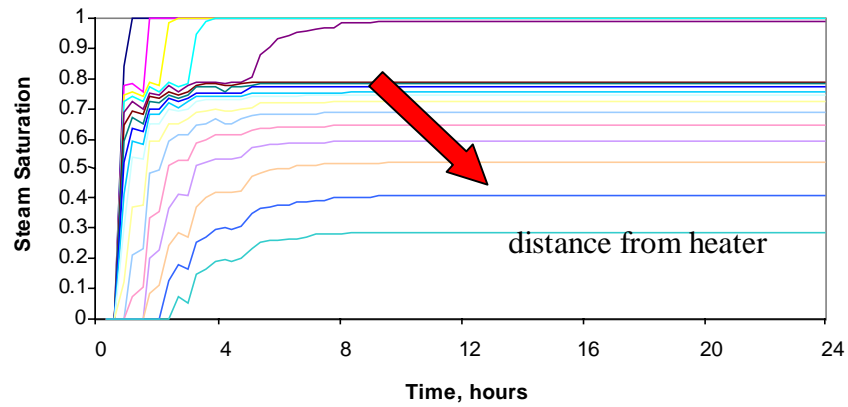


Figure 3.8a: Steam saturation profile at a constant heating rate = 3.5 W.

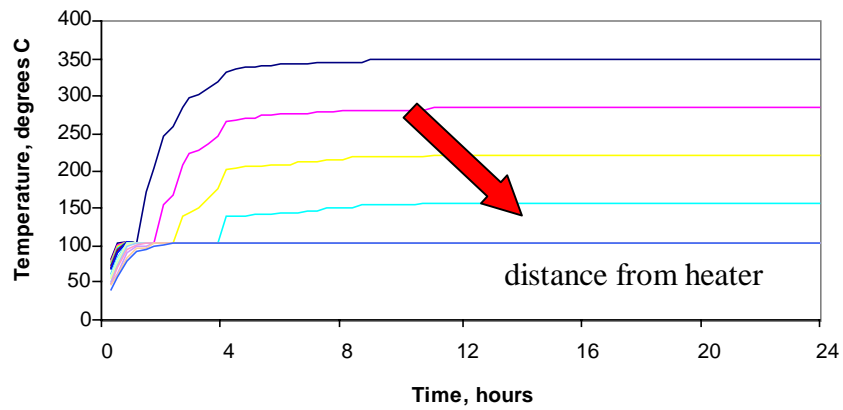


Figure 3.8b: Temperature profile at a constant heating rate = 3.5 W.

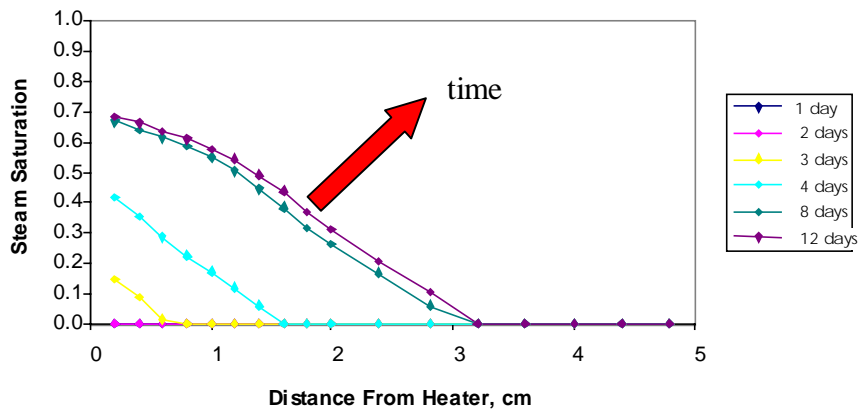


Figure 3.9: Steam saturation profile with distance at a constant heating rate = 2 W.

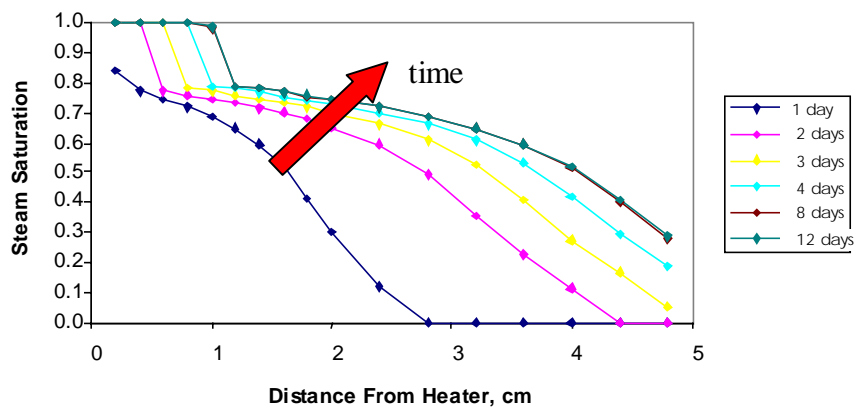


Figure 3.10: Steam saturation profile with distance at a constant heating rate = 3.5 W.

It is evident from the plots that the steam and two-phase regions expand as the heating rate is increased. At a constant heating rate equal to 1 Watt, liquid water in the core has not vaporized yet and temperatures are still below saturation temperatures. As the heating

rate is increased, boiling commences and steam and two-phase regions form. However, further increasing the heating rate resulted in convergence failures in the simulation runs. Temperatures in the steam region near the heater end approach very high values as the heating rate is further increased.

Steam saturation and temperature reach steady state values after approximately 12 hours of heating the core at a constant rate.

Figure 3.9 and 3.10 clearly indicate the evolution of an elbow in the steam saturation profile with time. During steady state at a constant heating rate equal to 3.5 Watts, the first centimeter of the core from the heater end is steam-filled. The steam saturation then abruptly drops to a value close to the assumed endpoint water saturation and stays close to this value within another centimeter. The steam saturation further goes down with distance from the heater end within the two-phase region.

The following charts are plots of the simulation results for the case of variable heating rates. Figure 3.11 shows the variable heating rates used by Guerrero et al. (1998) in their inverse modeling of the boiling experiments. The steady-state steam saturation profiles plotted in Figure 3.12 indicate two-phase conditions throughout the entire length of the core. No steam region and elbow in the steam saturation profile is evident from the simulation results.

The heating rates were further increased in the succeeding simulation runs to study the case when a steam region is formed. The heating rate as a function of time is shown in Figure 3.13 and the steam saturation profiles with time and distance are plotted in Figures 3.14 to 3.16. The boiling process was simulated using three different values of endpoint water saturation: 0.1, 0.2 and 0.5.

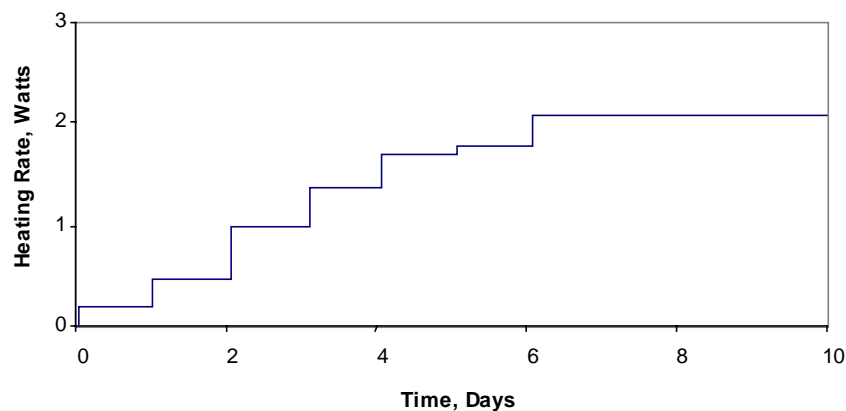


Figure 3.11: Heating rate as a function of time, Guerrero et al., 1998.

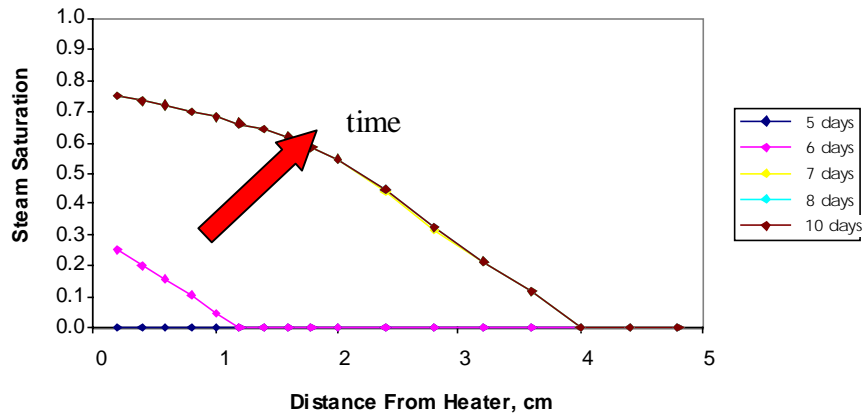


Figure 3.12: Steam saturation profile with distance: endpoint water saturation = 0.2.

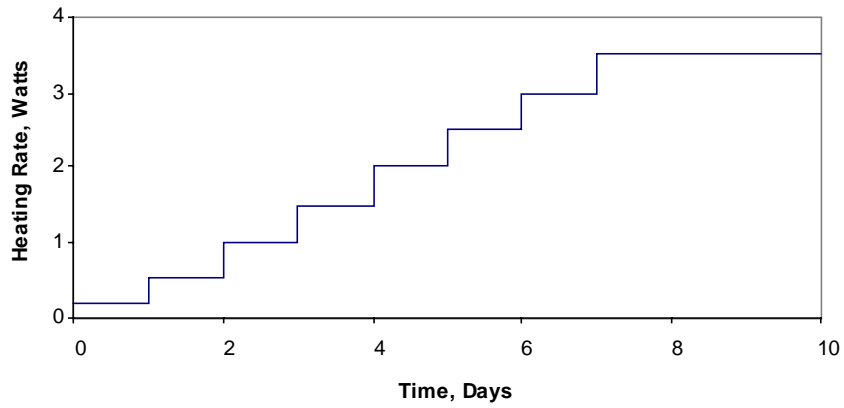


Figure 3.13: Heating rate as a function of time.

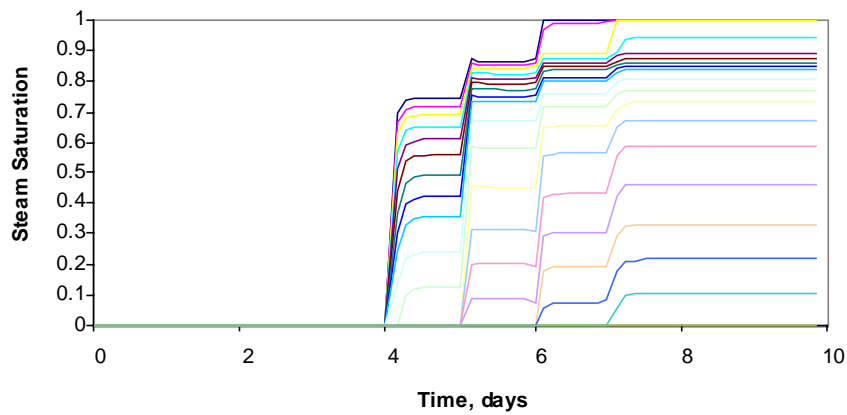


Figure 3.14a: Steam saturation profiles: endpoint water saturation = 0.1.

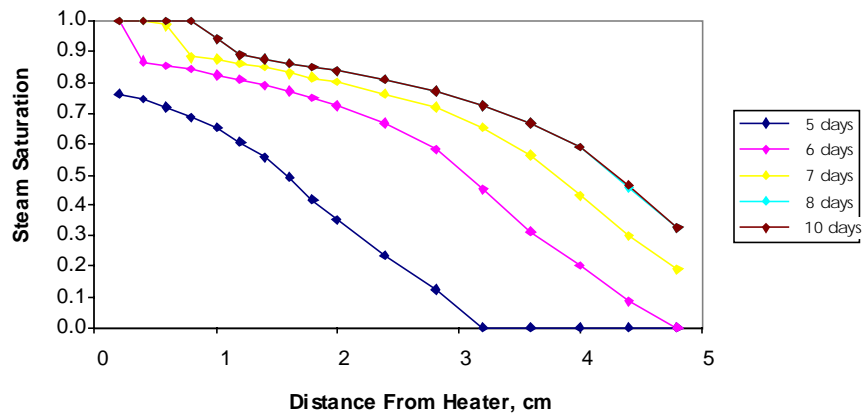


Figure 3.14b: Steam saturation profiles: endpoint water saturation = 0.1.

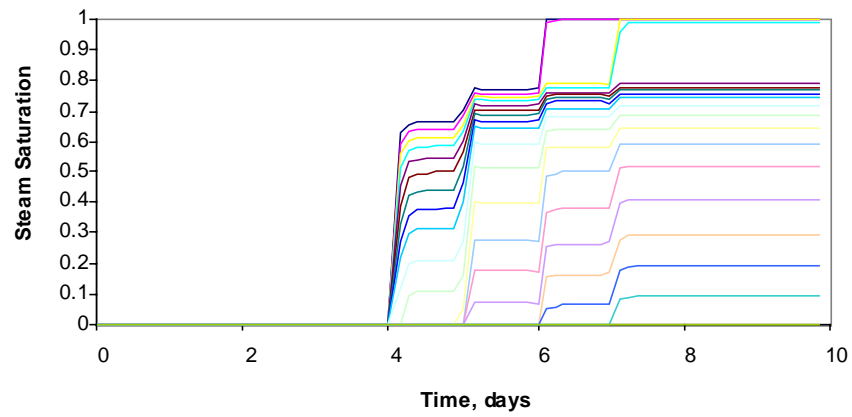


Figure 3.15: Steam saturation profiles: endpoint water saturation = 0.2.

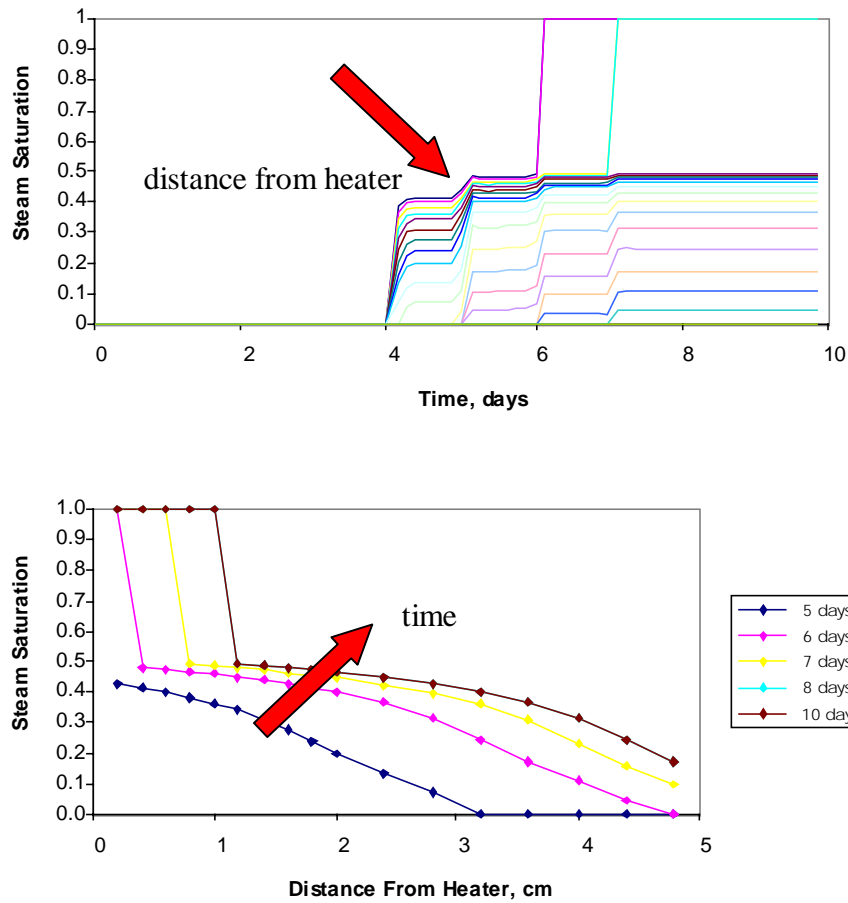


Figure 3.16: Steam saturation profiles: endpoint water saturation = 0.5.

The simulation results indicate a correlation between the elbow in the steam saturation profile and the endpoint water saturation. In all three cases, the steam region extends to a distance of one centimeter from the heater end. An abrupt drop in the steam saturation to a value close to the assumed endpoint water saturation then marks the transition to two-phase conditions corresponding to the elbow in the profile. The steam saturation stays close to this value behind the elbow and then further goes down with distance from the heater end.

This apparent correlation was not clearly evident in the simulation results presented in the previous quarterly report where a coarser grid model was used.

3.2.4 Future Work

Future work will involve analyzing the results of the boiling experiments performed by Satik and inferring the irreducible water saturation of Berea sandstone cores from the pressure, temperature and saturation data. Future work will also be directed toward designing boiling experiments using lower permeability geothermal reservoir rocks.

3.3 INFERRING ENDPOINT SATURATION FROM FIELD MEASUREMENTS

The discharge of saturated or superheated steam during the exploitation of vapor-dominated geothermal reservoirs greatly exceeds what can be stored as vapor. Therefore, vapor-dominated reservoirs must contain substantial amounts of liquid water to sustain production (James, 1968; Nathenson 1975; Grant, 1979). In describing the response of vapor-dominated reservoirs to exploitation, it is valid to assume that the liquid water is completely immobile. Although water may be slightly mobile in the natural state of the reservoir, it is soon immobile because the water saturation drops as fluids are produced (Grant, 1979). The liquid water is adsorbed in the pores of the reservoir matrix and is able to vaporize, but is not able to flow as liquid water.

Grant (1979) estimated the in-place water saturation of the Kawah Kamojang geothermal reservoir based on variations in the gas content of the production fluids. Changing the flow rate at the wellhead produces a response in the reservoir pressure and gas content, which allows for the estimation of the in-place water saturation or the endpoint water saturation of the reservoir rock. In contrast, this study aims to infer the endpoint saturations from field measurements of changes in the flowing enthalpies of producing wells.

Flow and lumped-parameter models can be used to describe the pressure, temperature and saturation distributions accompanying production. Grant used a flow model to infer the in-place water saturation of the Kawah Kamojang geothermal reservoir. In the previous quarterly report, a lumped-parameter or zero-dimensional model was used to infer reservoir saturations from changes in temperature and flowing enthalpy accompanying production. This study aims to build on this approach by extending the lumped-parameter model to consider transient, spatial and two-phase flow effects.

3.3.1 Flow Model

The flow of dry steam in vapor-dominated reservoirs can be described by the equations of the conservation of mass, energy and momentum. It is assumed that the immobile water does not impede the flow of steam and that the steam flow is governed by Darcy's law.

Mass Conservation:

$$\phi \frac{\partial}{\partial t} [S\rho_w + (1-S)\rho_s] = -\nabla \cdot (\vec{u}_s \rho_s) \quad (3.1)$$

Energy Conservation:

$$\frac{\partial}{\partial t} [(1-\phi)\rho_r U_r + \phi S\rho_w U_w + \phi(1-S)\rho_s U_s] = -\nabla \cdot (\vec{u}_s \rho_s H_s) \quad (3.2)$$

Momentum Conservation:

$$\bar{u}_s = -\frac{kk_{rs}}{\mu_s} \nabla p \quad (3.3)$$

Under reservoir conditions, the enthalpy of saturated steam is nearly constant with temperature. This approximation results in a simplified relation between pressure and saturation at any point in the reservoir.

$$(1-\phi)\rho_r U_r + \phi S \rho_w (U_w - H_s) + \phi(1-S)\rho_s (U_s - H_s) = \text{constant} \quad (3.4)$$

Reduction in the reservoir pressure resulting from production is accompanied by a reduction in reservoir temperature to maintain saturation conditions. Heat must then be mined from the rock to cool it, which is done by vaporizing some of the liquid water to steam. Therefore, a decline in the reservoir pressure results in a decline in the reservoir saturation. This mining of heat and consequent decline in saturation continues as long as saturation conditions exist. The saturation falls to zero at dry out conditions and the in-place water saturation can then be estimated using the initial and dry out reservoir conditions (Grant 1979).

$$\phi S_o = \frac{(1-\phi)\rho_r C_r (T_o - T_d)}{[\rho_w (H_s - H_w)]_{T_o}} \quad (3.5)$$

3.3.2 Variations in Gas Content

Variations in pressure and saturation in the reservoir during exploitation result in the transfer of mass between phases and, consequently, variations in the gas content of the liquid and vapor phases. The changes are determined by the equation for the conservation of gas (Grant, 1977).

Gas Conservation:

$$\phi \frac{\partial}{\partial t} [S \rho_w n_w + (1-S)\rho_s n_s] = k \nabla \cdot \left(\frac{n_s}{v_s} \nabla p \right) \quad (3.6)$$

Using a flow model, Grant (1979) showed that the variations in gas content with flow rate could be described using a parameter ζ , which depends on gas, steam and reservoir properties. The transient response in the gas content of the steam produced when a well is opened at time $t = 0$ to a flow rate W kg/s is given by

$$\ln \left(\frac{n_s}{n_{s_o}} \right) = - \int_0^\infty \frac{\zeta \exp(-\xi)}{\xi + \zeta \exp(-\xi)} d\xi \quad (3.7)$$

$$\zeta = \frac{W}{4\pi kh} \frac{\mu c_t}{\gamma} \quad (3.8)$$

$$\gamma = (1 - S)\rho_s + AS\rho_w \quad (3.9)$$

$$A = \frac{n_w}{n_s} \quad (3.10)$$

The in-place water saturation can then be inferred from gas data by considering the difference in the response of two gases with production. However, this method is valid only if the total amount of gas is small and each gas obeys Equation 3.7 independently with a different ζ parameter. After further simplification, Grant (1979) showed that the logarithm of the concentration of gas 1 in steam is a linear function of the logarithm of the concentration of gas 2 in steam. The slope of the straight line gives the water saturation of the reservoir rock.

$$\text{slope of } \ln(n_{s_1}) \text{ vs } \ln(n_{s_2}) \text{ plot} = \frac{(1 - S)\rho_s + A_2 S\rho_w}{(1 - S)\rho_s + A_1 S\rho_w} \quad (3.11)$$

3.3.3 Lumped-Parameter Model

On the other hand, the in-place water saturation can be estimated by solving simultaneously the mass and energy conservation equations that describe a lumped-parameter or zero-dimensional model of the reservoir.

Mass Conservation:

$$\Delta(\phi V\rho_w S) + \Delta(\phi V\rho_s [1 - S]) + m' = 0 \quad (3.12)$$

Energy Conservation:

$$\Delta(\phi V\rho_w S h_w) + \Delta(\phi V\rho_s [1 - S] h_s) + (1 - \phi)V\rho_r C_r \Delta T + m' h' = 0 \quad (3.13)$$

A plot of the flowing enthalpy of the production fluids as a function of the decline in reservoir pressure and the in-place water saturation can be obtained using this lumped-parameter model. This plot can be used as a diagnostic tool for estimating reservoir saturation based on production enthalpy and reservoir pressure data.

Consider as an example reservoir data from the Geysers geothermal field. The reservoir temperature based on shut-in downhole temperatures is about 240 °C. The porosity of the reservoir rock is 5%, rock density is 1,750 kg/m³ and rock specific heat is about 1 kJ/kgK. Figure 3.17 is a plot of the enthalpy and reservoir pressure drop as a function of the in-place water saturation.

The simple lumped-parameter model of the reservoir can, therefore, be used to estimate the irreducible water saturation of geothermal reservoir rocks using field measurements of temperature and flowing enthalpy. Consider a Geysers well that produces 200°C dry saturated steam. Based on the lumped-parameter model of the Geysers geothermal field, the in-place water saturation is about 0.5, which corresponds to the irreducible water saturation of the reservoir rocks since the well is producing dry saturated steam.

3.3.4 Future Work

The lumped-parameter approach does not take into account pressure and enthalpy variations with time and distance. The model assumes that the reservoir has a uniform saturation and temperature. Future work will involve modeling of two-phase radial flow to obtain pressure and saturation profiles with time and radial distance. Modeling results will provide a deeper insight on the estimation of reservoir saturation using field measurements. Furthermore, it is intended to extend this approach to liquid-dominated reservoirs that produce two-phase steam. The goal is to extrapolate the irreducible water saturation of the reservoir rocks using temperature and flowing enthalpy data.

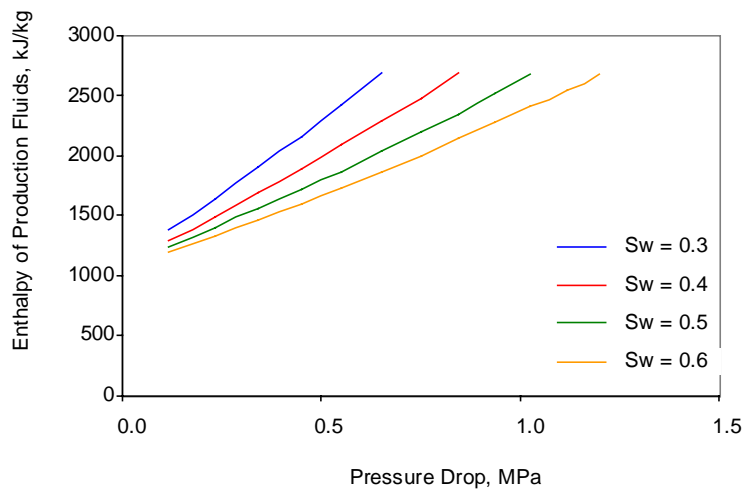


Figure 3.17: Enthalpy of production fluids as a function of reservoir pressure drop and in-place water saturation.

4. STEAM-WATER CAPILLARY PRESSURE

This research project is being conducted by Research Associate Kewen Li and Professor Roland Horne. The final objective of this project is to find a method for measuring steam-water capillary pressure in rocks. As a preliminary approach, we are studying the imbibition behavior of water into air-saturated rock.

4.1 INTRODUCTION

In the last quarterly report for January-March 1999, we reported a new theory developed for calculating air-water capillary pressure from the relationship between the imbibition rate and the reciprocal of recovery by water imbibition. This theory can be applied to steam-water-rock systems for measuring steam-water capillary pressures. The relationship between the imbibition rate and the reciprocal of recovery by water imbibition should be linear based on the new theory, which was confirmed by the experimental data in Berea with a permeability of about 600 md in the last quarterly report. This important behavior of water imbibition into air-saturated rock is not confirmed yet experimentally in rocks with low permeability (say less than 10 md) or unconsolidated porous media. Another essential issue we need to address is to compare the capillary pressure calculated using the new theory with the actual capillary pressure measured by some other reliable method. To this end, we will do the water imbibition test in a pack of glass beads positioned vertically and calculate the capillary pressure using the relationship between the imbibition rate and the reciprocal of recovery. The distribution of water saturation in the vertical direction will be measured using an X-ray CT scanner along the pack of glass beads. Therefore, the relationship between the water saturation and the height related to gravity will be measured. Based on the force balance between gravity and capillary pressure, the relationship between the water saturation and the height will be transferred into a capillary pressure curve.

In this quarter, we measured the properties of water imbibing into an air-saturated chalk with a permeability of about 5 md and in unconsolidated porous media (packs of glass beads and sands). The capillary pressure curve of a glass-bead pack was measured by using the X-ray CT technique. It was found from the experimental results that the relationship between the imbibition rate and the reciprocal of recovery by water imbibition was linear (as predicted by the theory) in both low permeable chalk and very highly permeable unconsolidated porous media (packs of glass beads and sands). These experimental results gave us a solid basis to infer air-water imbibition capillary pressure from the experimental data of water imbibition using the new theory developed in the last quarter.

4.2 THEORY

The basic mathematics was described in the last quarterly report for calculating air-water capillary pressure from the experimental data of water imbibition into air-saturated rocks. The relationship between the volume of water imbibed into the air-saturated rock and imbibition time could be measured during the imbibition experiments. The imbibition rate of water, defined as the volume or weight of water imbibition in unit time, was calculated

from this relationship and was then plotted versus the reciprocal of the water imbibition (volume or pore volume). The correlation between the imbibition rate and the reciprocal of recovery by water imbibition should be linear. The intersection at the y-axis (imbibition rate) of this line by linear regression may be used to calculate the effective water permeability; the slope of this line and the calculated effective water permeability may be used to calculate the air-water capillary pressure based on the new theory developed last quarter.

4.3 EXPERIMENTS

4.3.1 Fluids

To measure air-water capillary pressure in chalk, brine of 1.0 percent (wt) NaCl solution was used as the liquid phase and air the gas phase in the imbibition experiments. The brine had specific gravity and viscosity 1.01 and 1.0 cp at 20°C. For the packs of glass beads, distilled water was used as the liquid phase.

4.3.2 Core Samples

The permeability of the chalk sample was around 5 md; its length and diameter were 7.5 cm and 2.54 cm, respectively. The sand pack used had a gas permeability of about 5.8 darcy at a nitrogen flow rate of 200 ml/min; its length and diameter were 28.5 cm and 3.81 cm, respectively. A glass-bead pack was used for measuring air-water capillary pressure using the X-ray CT technique. This pack of glass beads had a gas permeability of about 25.7 darcy at a nitrogen flow rate of 200 ml/min; its length and diameter were 29.5 cm and 3.4 cm.

4.3.3 Apparatus

The equipment for measuring water imbibition into an air-saturated rock reported in the last quarterly report was modified to be able to do data acquisition automatically using the software LabView by National Instrument Company. A schematic of the apparatus is shown in Figure 4.1.

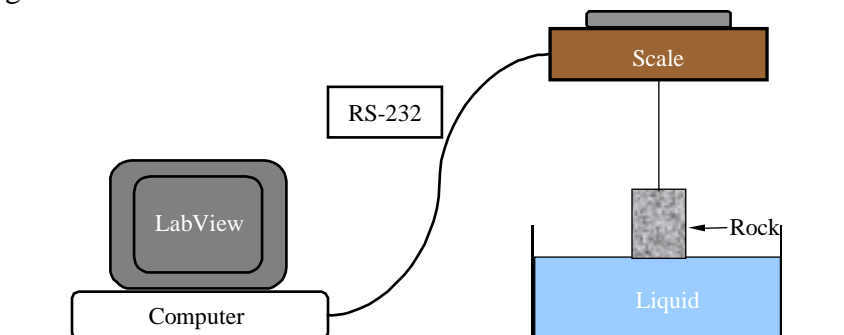


Figure 4.1: Schematic of apparatus for imbibition test.

The core sample was hung under a Mettler balance (Model PE 1600) which had an accuracy of 0.01g and a range from 0 to 1600 g. The water imbibed into the core was recorded in time by the balance using an under-weighing method and the real-time data

was measured continuously by a computer through an RS-232 interface. The purpose of the under-weighing method is to reduce the experimental error caused by water evaporation.

The structure of the glass-bead pack used in this study is shown in Figure 4.2. It is known on the basis of the new theory that we developed last quarter that the effect of the area at the bottom of the sample on imbibition rate is significant. In other words, the imbibition area of water should be equal to the cross-sectional area of the rock or the glass-bead sample. Experimentally, it was found (Schembre, et al., 1998) that there was a cone-shape distribution of water saturation at the bottom of a rock when water was introduced using a small tubing; this type of heterogeneous water distribution would cause error in calculating the capillary pressure. Therefore it is important to design the structure of the glass-bead pack so as to enable all the bottom part of the sample to contact water. For this purpose, a lot of holes were drilled at the bottom of the glass cylinder as shown in Figure 4.2.

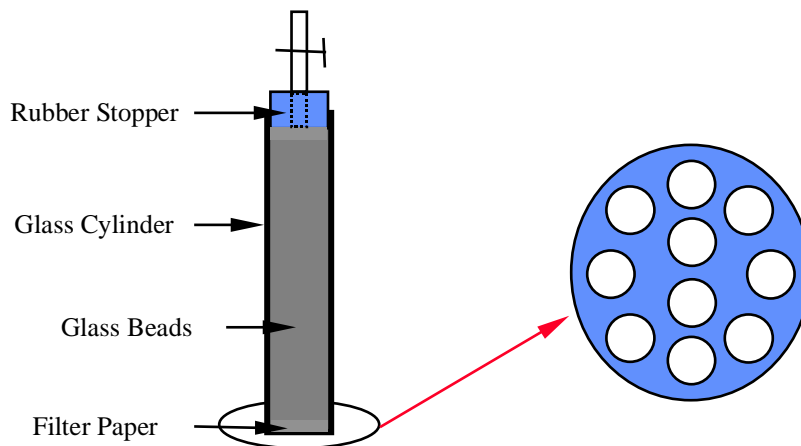


Figure 4.2: Schematic of the glass-bead pack.

Filter paper at the bottom of the glass cylinder was also helpful to avoid the formation of the cone-shape water distribution.

The CT-Scanner used in this study was a PickerTM 1200 SX X-ray CT scanner with 1200 fixed detectors. The voxel dimension is 0.5 mm by 0.5 mm by 5 mm, the tube current used in this study was 50 mA, and the energy level of the radiation was 140 keV. The acquisition time of one image is about 3 seconds while the processing time is around 40 seconds.

4.3.4 Procedure

Chalk was dried by heating it at a temperature of 85°C in an oven until its weight did not vary during eight hours. The core sample was assembled in the apparatus as shown in Figure 4.1 after it was cooled down. Water started to imbibe into the core when the bottom was brought in contact with the water surface by raising the water container. The

weight change of the core sample was then recorded with time and used to calculate capillary pressure.

Before packing, glass beads were dried by heating at a temperature of 85°C in an oven until their weight did not vary during eight hours. The glass beads were then packed into a glass cylinder as shown in Figure 4.2. Following that, a dry X-ray CT scan was made at each centimeter along the glass-bead pack that was positioned vertically. After that, the water imbibition test was conducted. An X-ray CT scan was made again at each centimeter along the glass-bead pack when the water stopped imbibing into the glass-bead pack to obtain the distribution of CT values. Finally, the glass-bead pack was dried and another X-ray CT scan was made after completely resaturating with water. The CT values measured from the three X-ray CT scans were used to calculate the porosity and the distribution of the water saturation as a function of height.

4.4 RESULTS

Figure 4.3 shows the results of water imbibition into the air-saturated chalk. The amount of water imbibition increases with time. It can be seen from Figure 4.3 that the imbibition was almost finished when the water imbibition front reached the top of the rock. This may be evidence that the imbibition front is a piston-like front with constant water saturation. This implies that the water saturation behind the imbibition front is almost constant.

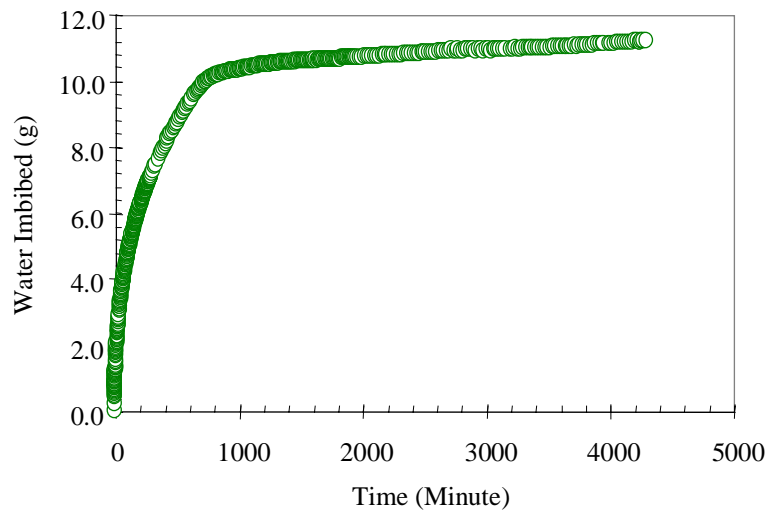


Figure 4.3: Water imbibition vs. time in chalk.

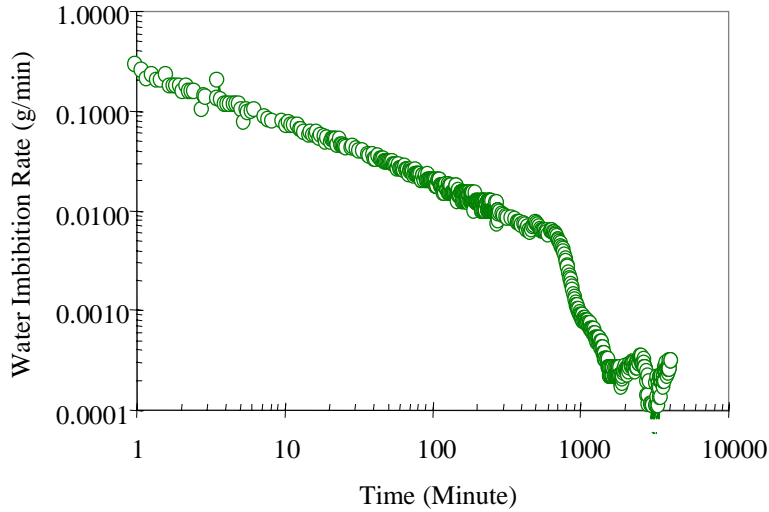


Figure 4.4: Water imbibition rate vs. time in chalk.

The relationship between the water imbibition rate and the time is plotted in Figure 4.4. An interesting phenomenon in Figure 4.4 is that the relationship between water imbibition rate and time is nearly linear on a log-log plot until the water imbibition front reached the top of the rock.

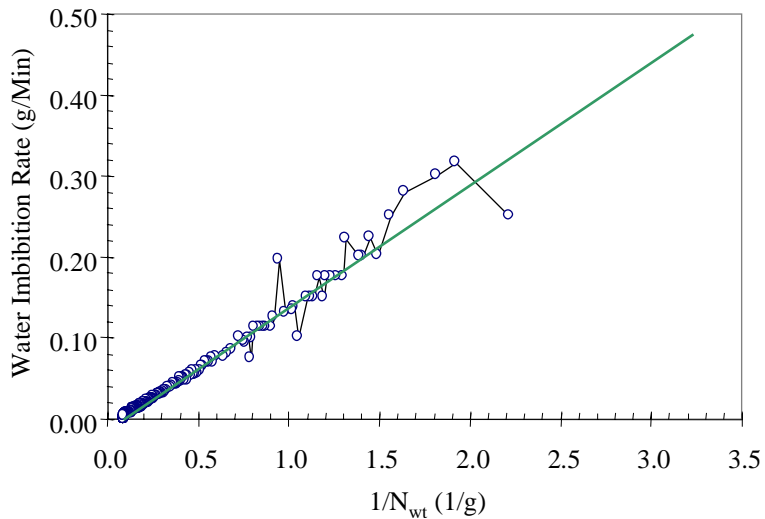


Figure 4.5: Water imbibition rate vs. reciprocal of production in chalk.

The water imbibition rate vs. the reciprocal of production (or the weight of water imbibed into the rock) is shown in Figure 4.5. Figure 4.5 demonstrates that the relationship between the water imbibition rate and the reciprocal of production is also linear in chalk as predicted by the theory developed last quarter.

One water imbibition test was conducted in an air-saturated sand pack with a gas permeability of about 5.8 darcy measured at 200ml/min using nitrogen. Figure 4.6 shows the results of water imbibition into the sand pack.

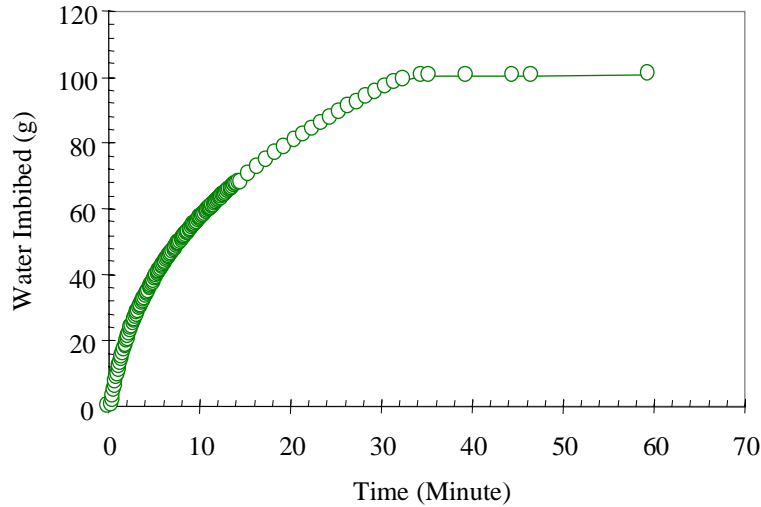


Figure 4.6: Water imbibition vs. time in a sand pack.

It can also be seen from Figure 4.6 that the imbibition of water into a sand pack was almost finished when the water imbibition front reached the top of the sand pack. This may demonstrate that water imbibition front is also a piston-like front with constant water saturation. This also shows that the water saturation behind the water imbibition front is almost constant in a sand pack.

The relationship between the water imbibition rate and the time is plotted in Figure 4.7.

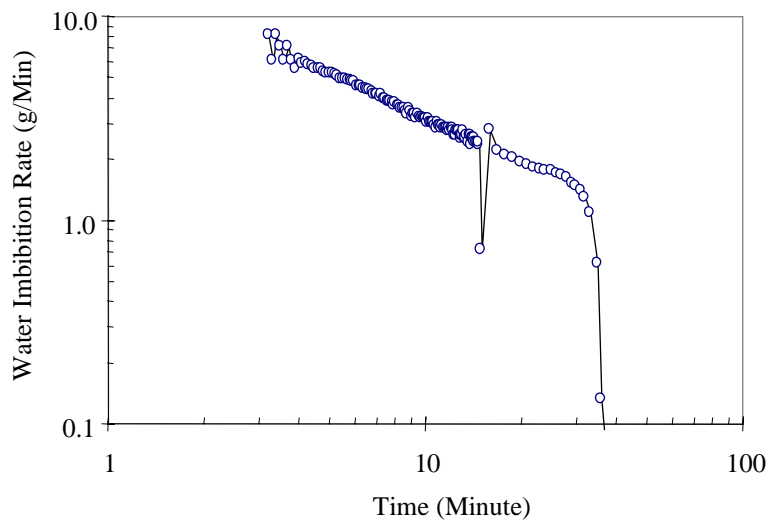


Figure 4.7: Water imbibition rate vs. time in a sand pack.

The imbibition rate of water into an-air saturated sand pack is very high as shown in Figure 4.7. It is observed in this figure that the relationship between the water imbibition rate and time in a sand pack is nearly linear on a log-log plot, which is similar to the behavior observed in chalk (see Figure 4.4).

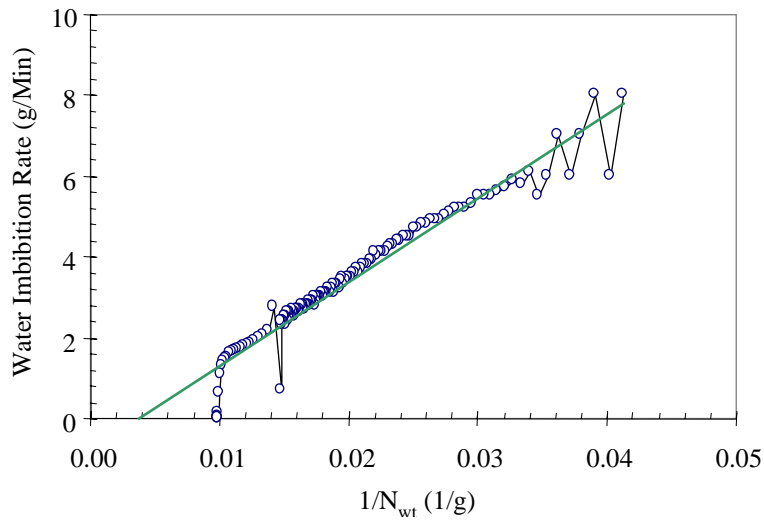


Figure 4.8: Water imbibition rate vs. reciprocal of production in a sand pack.

The water imbibition rate vs. the reciprocal of production is shown in Figure 4.8. The y-axis is the water imbibition rate and x-axis the reciprocal of production represented by N_{wt} . This figure also demonstrates that the relationship between the water imbibition rate and the reciprocal of production in a sand pack (unconsolidated porous medium) is linear as predicted by the theory developed last quarter. The purpose of this experiment was to compare the measured capillary pressure at zero water saturation with the capillary pressure calculated using the new theory using water imbibition rate. The capillary pressure at zero water saturation can be measured by the height of the water imbibition in the sand pack if the height is less than the length of the sand pack. Unfortunately, in this sand pack the height of water imbibition was longer than the length of the sand pack.

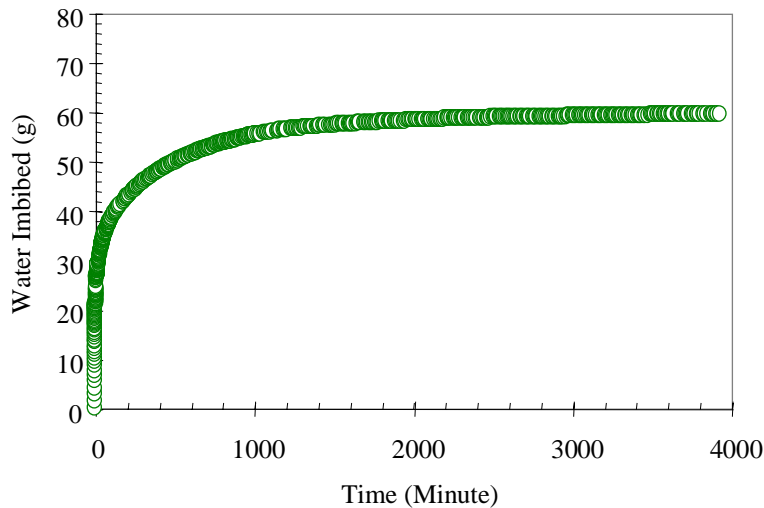


Figure 4.9: Water imbibition vs. time in a glass-bead pack.

One water imbibition test was run in a glass-bead pack after the sand pack test. The size of glass beads was 90 mesh; the gas permeability measured at a flow rate of 200 ml/min using nitrogen was about 25.7 darcy. Figure 4.9 shows the water imbibition into the glass-bead pack as a function of time.

The relationship between the water imbibition rate into the air-saturated glass-bead pack and the experimental time is plotted in Figure 4.10. The water imbibition rate vs. the reciprocal of the production is plotted in Figure 4.11.

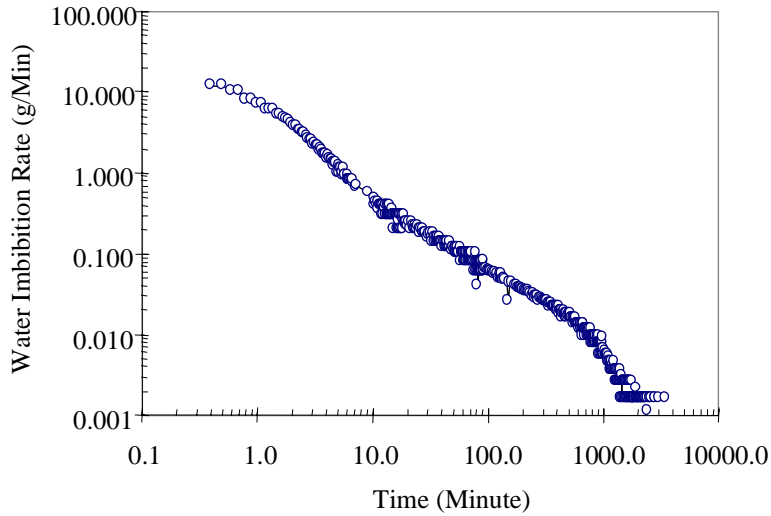


Figure 4.10: Water imbibition rate vs. time in a glass-bead pack.

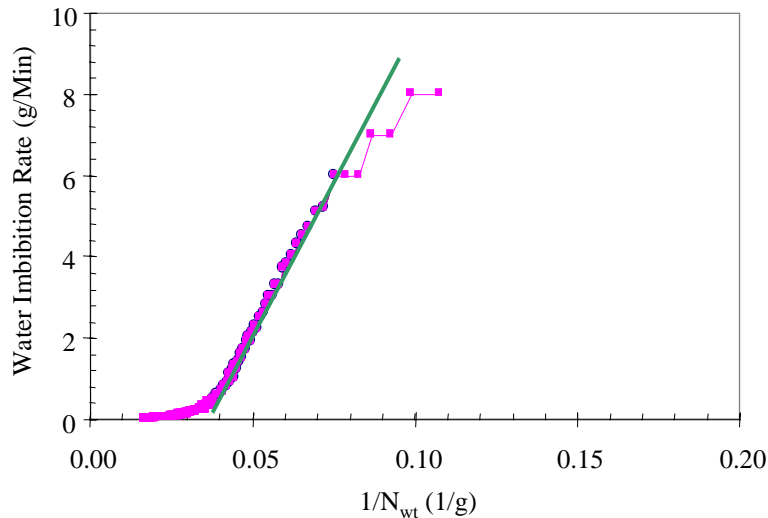


Figure 4.11: Water imbibition rate vs. reciprocal of production in a glass-bead pack.

It can be seen from Figure 4.11 that the relationship between the water imbibition rate and the reciprocal of production in the glass-bead pack (unconsolidated porous medium) is also linear over a period of imbibition process as predicted by the theory developed last quarter. At the initial stage of water imbibition, it is usually difficult to measure accurately

the amount of water imbibed into the glass-bead pack or rock due to the influence of the buoyancy caused by inserting the bottom of the sample into the water. There may be some error although the effect of buoyancy on the data acquisition was calibrated by weighing the sample after the water imbibition test. When the water imbibition front reached a certain height in the glass-bead pack, the imbibition process might not be a capillary pressure dominated process as we assumed in the new method. The reason is that the effect of the gravity on the imbibition process increases with the increase of the height of the water imbibition front. This may explain why the relationship between the water imbibition rate and the reciprocal of production in a glass-bead pack is not linear at late time as shown in Figure 4.11.

With the application of the new theory developed in the last quarterly report, the imbibition capillary pressure at zero water saturation calculated using the linear relationship shown in Figure 4.11 is about 10 cm (water column). We will discuss the capillary pressure curve in the glass-bead pack measured by an X-ray CT scanner technique in the next section.

The distribution of the porosity of the glass-bead pack from the bottom to the top is shown in Figure 4.12. This figure shows that the porosity distribution was not so uniform. The average porosity measured by the X-ray CT method is about 38.0%, which is consistent with the value 38.6% measured by the routine saturation method.

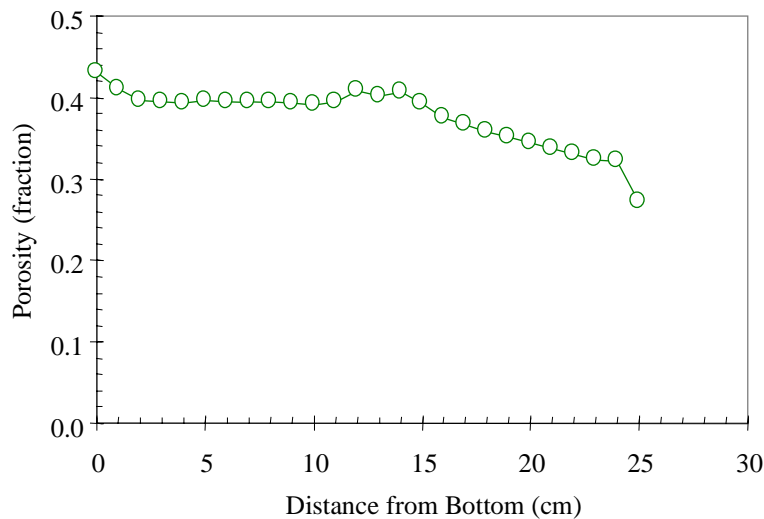


Figure 4.12: Porosity distribution in a glass-bead pack.

The distribution of CT values before and after the water imbibition test is shown in Figure 4.13. CT_{dry} in this figure represents the CT value of the glass-bead pack when the sample is air-saturated and $CT_{objective}$ represents the CT value of the glass-bead pack after the water imbibition was finished. The height in the pack at the point where the value of CT_{dry} is equal to the value of $CT_{objective}$ should represent the capillary pressure at zero water saturation (see Figure 4.13). It can be seen from Figure 4.13 that the capillary pressure at zero water saturation in the glass-bead pack is about 20 cm of water column.

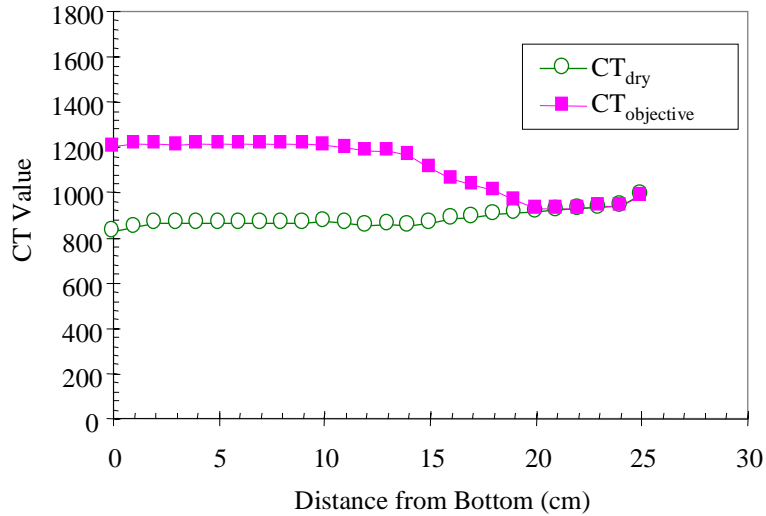


Figure 4.13: Distribution of CT values before and after imbibition test in a glass-bead pack.

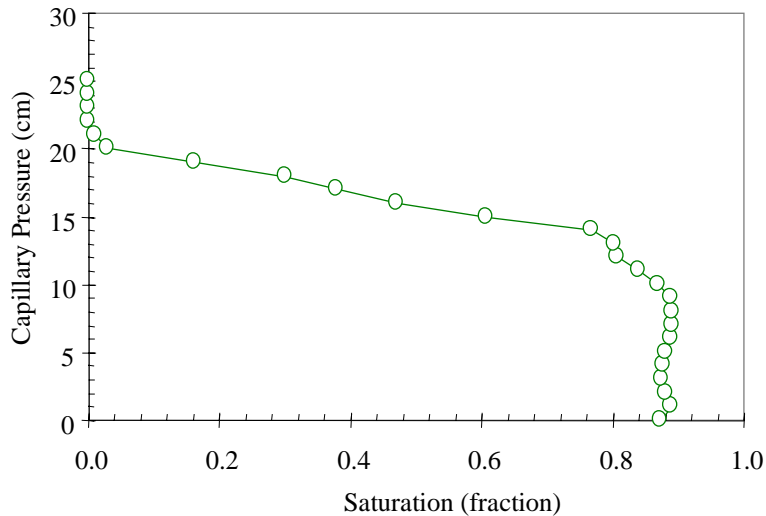


Figure 4.14: Air-water imbibition capillary pressure of a glass-bead pack measured using the X-ray CT technique.

The air-water imbibition capillary pressure curve of the glass-bead pack measured using the X-ray CT method is plotted in Figure 4.14. It can be seen from Figure 4.14 that the air-water imbibition capillary pressure at zero water saturation is about 20 cm (water column). The air-water imbibition capillary pressure at zero water saturation calculated using the new method is less than that measured by an X-ray CT technique. This might be brought about the moving of glass beads during the experiments. The moving of the glass beads would affect the CT values and the calculation of porosity and water saturation and hence the calculation of capillary pressure. We will repeat this experiment or use another technique to verify the new theory.

4.5 CONCLUSIONS

Based on the work performed this quarter, the following conclusions may be drawn:

1. The relationship between water imbibition rate and the reciprocal of the production is linear in both low permeable chalk and high permeable unconsolidated porous media (sand and glass-bead packs).
2. The air-water imbibition capillary pressure at zero water saturation calculated using the new method developed last quarter is less than that measured by the X-ray CT technique in a glass-bead pack.
3. An apparatus for implementing liquid imbibition test with automatic data acquisition function using the software LabView was developed.

4.6 FUTURE WORK

We will repeat the measurement of the air-water capillary pressure curve and the water imbibition test in the glass-bead pack. We are studying the water imbibition behavior in air-water systems at different initial water saturations and calculating the capillary pressure in order to verify further the feasibility of this new method.

5. ACCURATE MEASUREMENT OF STEAM FLOW PROPERTIES

This research project is being conducted by Research Associate Kewen Li and Professor Roland Horne. The aim of this project is to study the effect of gas slippage on steam-water relative permeabilities.

5.1 SUMMARY

The results of Satik reported in early 1998 showed the unexpected phenomenon that the steam phase relative permeabilities at some water saturations may be significantly greater than one. In the quarterly report for January-March 1999 these results were explained physically as being due to the Klinkenberg slip effect. The phenomenon was reproduced in nitrogen-brine flow using a new method developed for measuring and correcting gas relative permeabilities. In the current quarter, a new apparatus was constructed for measuring the slip factor in steam. The slip factor for steam flow in Berea was measured using the new apparatus and used to correct the previously measured steam phase relative permeabilities. It was found that all the steam phase relative permeabilities calibrated using the measured steam slip factor became less than one. The effect of temperature on the values of slip factor of both nitrogen and steam was also investigated with temperatures up to 150°C. Experimental results demonstrated that there was significant effect of temperature on the slip factors of both nitrogen and steam. This implies that steam slip factor should be measured at the temperature at which the steam relative permeabilities are measured.

5.2 INTRODUCTION

It is known that the gas slip factor depends on temperature, the type of gas, and rock properties. In the previous quarter, we studied the gas slip behavior of nitrogen in single- and two-phase gas-liquid flow at room temperature. In the current quarter, we focused on the gas slippage of both nitrogen and steam at higher temperatures. To this end, we developed a new apparatus for measuring the slip factor of steam at different temperatures and pressures. This apparatus was also designed to measure the end-point relative permeabilities of steam at residual water saturations.

5.3 EXPERIMENTS

5.3.1 Fluids

Distilled water was used to generate steam needed for the measurement of steam permeability; the specific gravity and viscosity were 1.0 and 1.0 cp at 20°C. The steam properties at high temperatures were calculated. In comparison experiments, nitrogen was used as the flowing gas.

5.3.2 Core Samples

The Berea core used in this study for measuring steam and nitrogen slip factors at high temperatures was the same as that described in the last quarterly report. The permeability

and porosity of the rock were 1280 md and 23.4%, respectively; the length and diameter were 43.2 cm and 5.08 cm.

5.3.3 Apparatus

Figure 5.1 shows a schematic of the apparatus developed for measuring the steam slip factor and the gas slip factor of nitrogen at high temperatures. The steam generator was a heater with a power of 500 W. The power required to generate steam was roughly calculated according to the flow rate of water injection and the temperatures of water and steam and then applied to the steam generator. For making sure that the injected cold water was generated to steam, a coil of stainless steel tubing with a length of about 2 m was installed between the steam generator and the inlet of the core in the oven. The balance (Model BP6100) in Figure 5.1 was manufactured by Sartorius Corporations and used to monitor the water saturation in the core sample; this balance has an accuracy of 0.1g and a range from 0 to 6100 g.

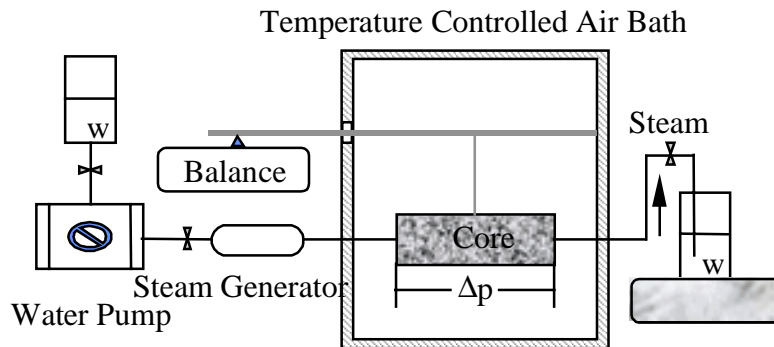


Figure 5.1: Schematic of steam slip factor test.

The pump (Model III) used to inject distilled water was manufactured by ConstaMetric; the minimum pumping flow rate is 0.1 ml/min with an accuracy of 1%. This pump is a constant-rate pump; its flow rate was calibrated before the experiment using a stop watch and a Mettler balance (Model PE 1600) with an accuracy of 0.01g and a range from 0 to 1600 g. The comparison curve of flow rate for this pump at room temperature is shown in Figure 5.2. The measured flow rates were consistent with those specified on the pump.

The flow rate of steam can be calculated using the water injection rate and the density of steam at the temperature and pressure measured during the experiment.

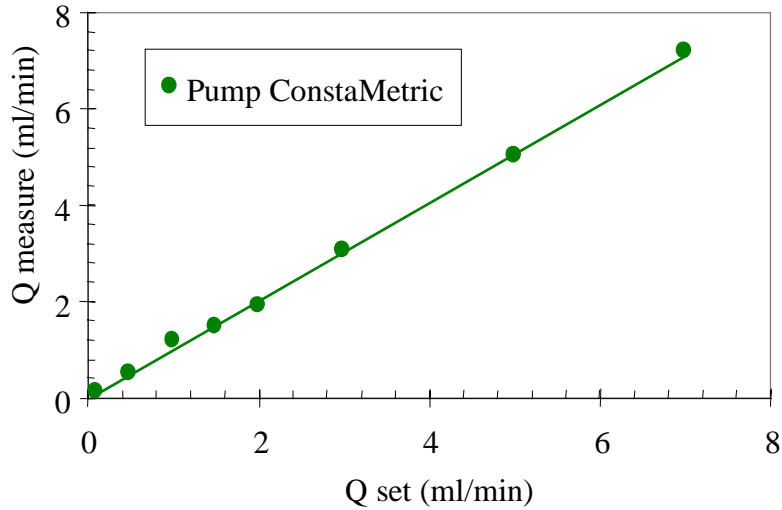


Figure 5.2: Calibration of flow rate for ConstaMetric pump.

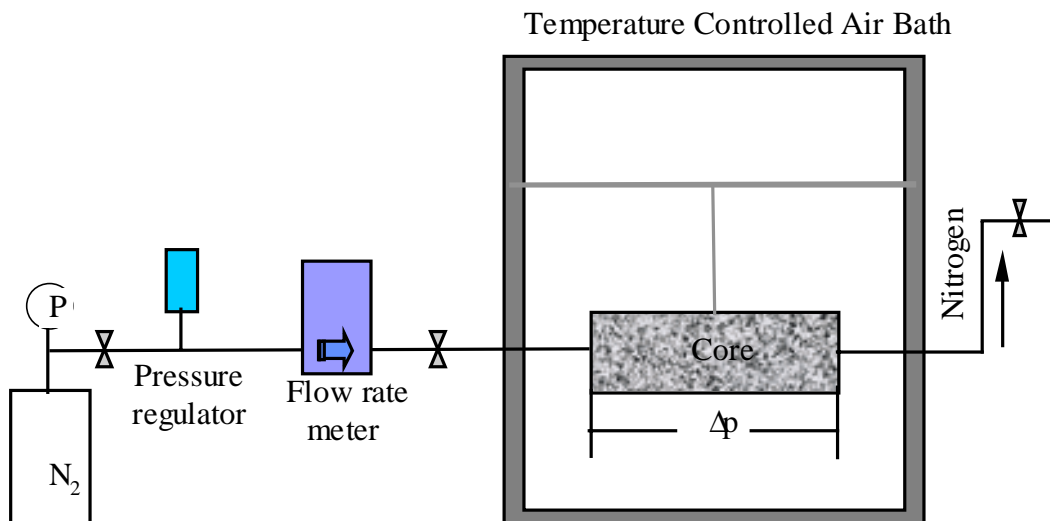


Figure 5.3: Schematic of nitrogen slip factor experiment at high temperatures.

The apparatus for measuring gas slip factor of nitrogen at high temperatures is shown in Figure 5.3. The flow rate of nitrogen was measured outside the high temperature oven by a mass flow transducer (also a flow rate controller) manufactured by Matheson Company. This mass flow rate meter and controller (Model 8272) has an accuracy of 1% in a range from 0 to 2000 ml/min. The calibration curves of flow rate for this mass flow transducer using both air and nitrogen are shown in Figure 5.4. There is almost no difference between the flow rates using air and nitrogen. In Figure 5.4 the x-axis represents the flow rates read or set on the controller for the mass flow transducer and y-axis the flow rates measured using a stop watch and the volume of water displaced by gas in a vertical glass

cylinder at room temperatures. Over a range of 0 to 2000 ml/min, we could set the flow rate of nitrogen as necessary using the mass flow controller and transducer before the experiments. The flow rate of nitrogen during the experiment was automatically controlled and kept at the value set before the experiment. The flow rates of nitrogen at room temperature were calibrated using the equation shown in Figure 5.4 and then the flow rates at the experimental temperatures were calculated using the equation of state for ideal gases in order to compute the gas permeabilities at the experiment temperature.

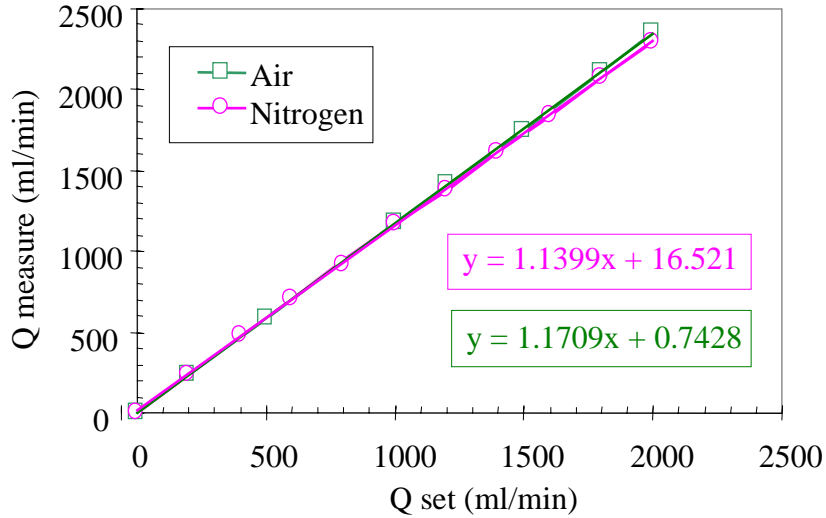


Figure 5.4: Calibration of flow rate for mass controller and transducer (Model 8272).

The differential pressure across the core sample was measured using a differential pressure transducer manufactured by Celesco Company; this transducer (Model DP30) has a linearity of 0.5% and a repeatability of 0.5% full scale. The diaphragm used in this study has a range from 0 to 10 psi. This differential pressure transducer was checked using a pressure gauge with an accuracy of 0.1 psi. Figure 5.5 plots the measured data.

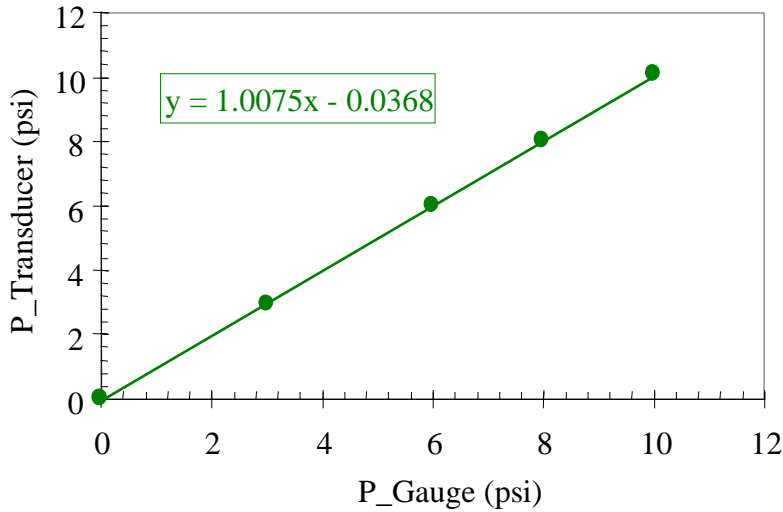


Figure 5.5: Calibration of differential pressure transducer.

The x-axis in Figure 5.5 is the pressure measured by the pressure gauge and y-axis the pressure measured by the transducer. It can be seen from Figure 5.5 that the measured data of pressure are in good agreement.

The coreholder and the method to assemble the core sample used in this study were similar to those of Satik and Horne (1998).

5.3.4 Procedure

The core was first dried by evacuation. The weight of the coreholder was monitored using a Sartorius balance with an accuracy of 0.1 g. The core was assumed to be dry when the weight did not change in eight hours of evacuation at a vacuum of about 30 millitorr. Then the gas permeabilities were measured at different mean pressures using nitrogen at room temperature. The mean pressures in the core were varied by changing the flow rates of nitrogen with the Matheson mass flow controller. Following that, the core was heated gradually to the experiment temperature and then the nitrogen permeabilities were measured again at that temperature. The nitrogen slip factor at different temperatures was calculated using the measured permeabilities as a function of mean pressure.

After the measurement of nitrogen slip factor at different temperatures, the core was evacuated in order to remove the nitrogen and the injection of steam was then started at a temperature higher than 100°C. The steam permeabilities were measured at different mean pressures by varying the water injection rate when the differential pressure across the core was stabilized. It was found that it took less time for steam pressures to be stabilized at higher flow rates of injection. The saturation pressure at the experimental temperature was calculated and the maximum steam injection rate was then roughly computed using Darcy's equation. The steam injection rate needed to be less than the calculated maximum flow rate at that temperature. Following that, the core was heated up and the steam permeabilities were measured again at the higher temperature. The slip factor of steam was calculated using the measured steam permeabilities at different mean pressures.

5.4 RESULTS

Both nitrogen and steam slip factors at different temperatures were measured using the new apparatus. It was found that there was a significant effect of temperature on both steam and nitrogen slip factors.

Figure 5.6 shows the effect of temperature on nitrogen permeabilities and slip factors in Berea. The x-axis in Figure 5.6 is the mean pressure across the two ends of the core sample and y-axis the nitrogen permeabilities at different mean pressures and different temperatures. The temperature ranged from room temperature to about 120°C. It is seen from Figure 5.6 that the nitrogen permeabilities at specific pressures increase with temperature. The intrinsic permeabilities (at infinite mean pressure) at different temperatures are equal, at around 1200 md. This intrinsic permeability is close to but less than the absolute permeability measured by water flow.

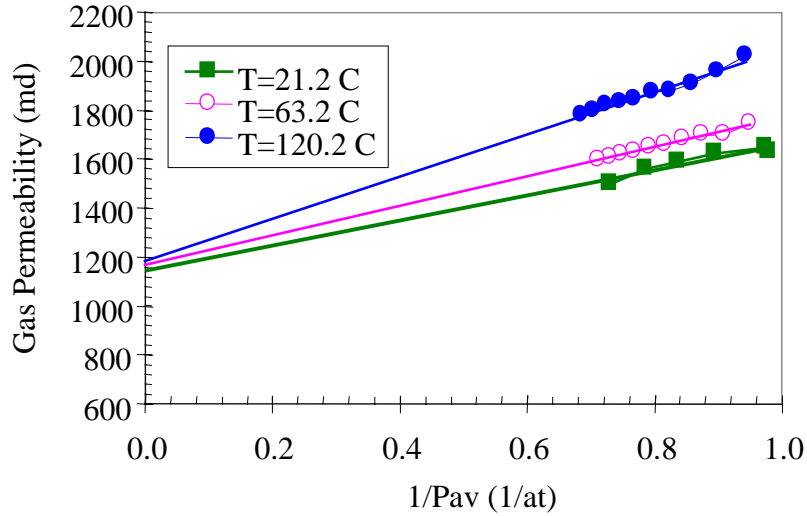


Figure 5.6: Effect of temperature on nitrogen permeabilities.

Figure 5.6 demonstrates that the nitrogen slip factor increases with temperature. These results are consistent with those reported by Wel et al. (1986); their measurements were made within a lower range of temperature from 0 to 63°C. The relationship between temperature and nitrogen slip factor is shown in Figure 5.7.

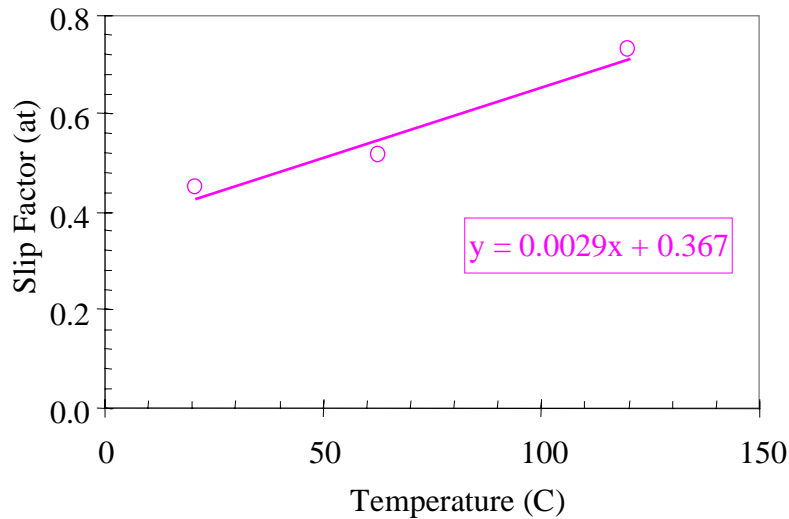


Figure 5.7: Effect of temperature on nitrogen slip factor.

The effect of temperature on steam permeabilities and slip factors in Berea are shown in Figure 5.8. The slip factor of steam was measured at two different temperatures (120.2°C and 150.8°C). It is seen from Figure 5.8 that the steam permeabilities at specific pressures increase with temperature. The intrinsic permeabilities of steam at the two different temperatures are roughly equal to each other, at around 700 md. This intrinsic permeability, however, is less than the absolute permeability measured by water flow.

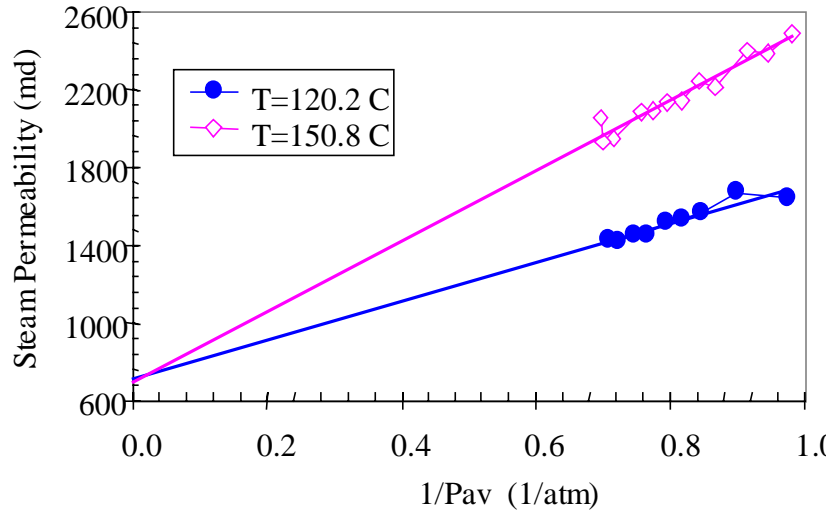


Figure 5.8: Effect of temperature on steam permeabilities and slip factor.

The values of steam slip factor at temperatures of 120.2°C and 150.8°C are 2.6 and 1.5 atm, respectively. The values may need to be confirmed by further experiments since the intrinsic permeabilities are not equal to the absolute permeability measured by water injection. However, it can be seen from Figure 5.8 that the value of steam slip factor at high temperature is greater than that at low temperature.

As shown in Figure 5.9, Satik and Horne (1998) observed an unexpected phenomenon in that the steam relative permeabilities at some water saturations sometimes appeared to be greater than one (represented by open triangle in Figure 5.9). A similar phenomenon was also found in the recent experiments conducted by Mahiya (see Section 1). The steam relative permeabilities were corrected based on the steam slip factors measured here and shown in Figure 5.9 (represented by solid circle). The influence of water saturation on steam slip factor was neglected in the calibration due to the lack of experimental data. The value of the steam slip factor used in the calibration was 1.5 atm, which was the value measured at a temperature of 120.2°C. It can be seen from Figure 5.9 that the corrected steam relative permeabilities calibrated using the experimental mean pressure and the steam slip factor become less than one.

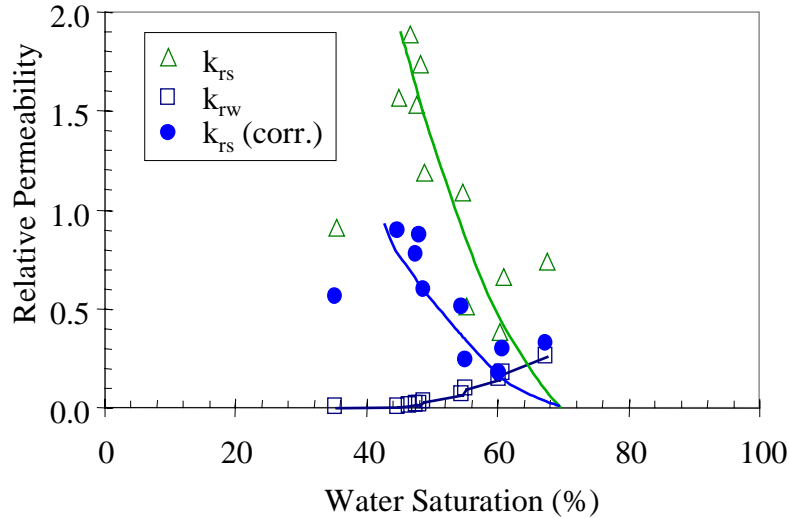


Figure 5.9: Calibration of steam permeabilities considering steam slippage.

5.5 DISCUSSION

It is known from our previous study (Li and Horne, 1999) that there is a significant effect of water saturation on the nitrogen slip factor in nitrogen-water two-phase flow in a certain range of water saturations. It is really a challenge to study the effect of water saturation on steam slip factor in steam-water flow. We have to measure the steam permeabilities at different mean pressures in order to calculate steam slip factor. The water saturation may change when the mean pressure is varied even at the same temperature. The essential issue is how to keep the water saturation constant while varying the mean pressure in the core system. It may be too difficult to do so. The suggested solution is in the following. We are planning to develop a new steady-state method to measure the relative permeabilities of steam and water. The main idea is to heat up the core saturated completely with water to a certain temperature (say 120°C) and keep the pressure at the core outlet at a certain value (say about 20 psig) using a back-pressure regulator while injecting water. The heat guards with an automatic control system will be used to make it possible for the experiments to be implemented under near-adiabatic conditions (Mahiya, 1999). The water in the core at the above temperature and pressure conditions should be in liquid state because the saturation pressure at 120°C is about 14.1 psig. The outlet pressure is then decreased under 14.1 psig and the inlet pressure is kept above 15 psig. Therefore, there may be a distribution of water saturation along the core from residual water saturation at outlet to 100 % at inlet. The relative permeabilities of steam and water could be calculated in the whole range of water saturation by just one test. The distribution of water saturation will be measured by an X-CT scanner technique (Ambusso, et al, 1996) and the distribution of pressure will be measured by differential pressure transducer at different position along the core after the steady-state is reached. This technique will be expected to reduce significantly the experimental time compared with the existing method (Ambusso, et al, 1996) for measuring steam-water relative permeabilities and make it possible to study the effect of water saturation (mobile and

immobile) on steam slip factor. The main procedure is in the following. After the relative permeabilities of steam and water are measured at one mean pressure using the new technique, the measurement will be repeated at different mean pressures that could be varied by using the back-pressure regulator at the core outlet. Therefore we could calculate the steam relative permeabilities at different water saturations and different mean pressures. The steam slip factor at different water saturations may be calculated by this technique.

5.6 CONCLUSIONS

Based on the present work, the following conclusions may be drawn:

1. Steam slippage is significant even in a high permeable rock and may be needed to take into account for calculating steam relative permeabilities in steam-water flow.
2. All the steam phase relative permeabilities calibrated using the gas slip theory in gas-liquid two-phase flow through porous media with the measured steam slip factor were less than one.
3. Neglecting the steam slip effect in a steam-water two-phase flow may overestimate steam relative permeabilities and hence overestimate the productivity of geothermal wells.
4. The effect of temperature on the steam slip factor is also significant. The steam slip factor increases with an increase of temperature.
5. A new apparatus has been developed for measuring steam slip factor and steam relative permeabilities at residual water saturations.
6. The steam relative permeabilities calibrated using the new concept with steam slip factor are of importance in reservoir engineering, numerical simulation, and for applying the experimental results at the geothermal reservoir scale.

5.7 FUTURE WORK

We will repeat the measurement of steam slip factor using a similar core and coreholder to confirm the value of the steam slip factor. We will also start to measure relative permeabilities of steam and water using the new technique that is described in the section of discussion.

6. REFERENCES

- Ambusso, W.J.: *Experimental Determination of Steam-Water Relative Permeability Relations*, MS report, Stanford University, Stanford, California (1996).
- Ambusso, W., Satik, C., and Horne, R.: "A Study of Relative Permeability for Steam-Water Flow in Porous Media", Proceedings of 21st Workshop on Geothermal Reservoir Engineering, Stanford University, Stanford, California (1996).
- Ambusso, W., Satik, C., and Horne, R.N.: "Determination of Relative Permeability for Steam-Water Flow in Porous Media," paper SPE 36682, presented at the 1996 Annual Technical Conference and Exhibition, Denver, Colorado, Oct. 6-9.
- Arihara, N.: *A Study of Non-Isothermal Single and Two-Phase Flow Through Consolidated Sandstones*, PhD dissertation, Stanford University, Stanford, California (1976).
- Bodvarsson, G.S., O'Sullivan, M.J., and Tsang, C.F.: The Sensitivity of Geothermal Reservoir Behavior to Relative Permeability Parameters, *Proceedings*, 6th Workshop on Geothermal Reservoir Engineering, Stanford, CA, Dec. 16-18, 1980.
- Chen, J.K., Council, J.R., and Ramey, H.J., Jr.: Experimental Steam-Water Permeability Curves," *GRC Trans.* **2** (1978), pp 102-104.
- Clossman, P.J., and Vinegar, J.J.: "Relative Permeability to Steam and Water at Residual Oil in Natural Cores; CT Scan Saturation," SPE paper 17449.
- Corey, A.T.: The Interrelations Between Gas and Oil Relative Permeabilities, *Producers Monthly* **19** (1954), pp 38-41.
- Council, J.R., and Ramey, H.J., Jr.: Drainage Relative Permeabilities Obtained from Steam-Water Boiling Flow and External Gas Drive Experiments, *GRC Trans.* **3** (1979), pp 141-143.
- Grant, M.A.: Permeability Reduction Factors at Wairakei, *Proceedings*, AIChE-ASME Heat Transfer Conference, Salt Lake City, Utah (August 1977), pp 15-17.
- Grant, M.A.: "Water Content of the Kawah Kamojang Geothermal Reservoir", *Geothermics*, Volume 8, (1979) pp 21-30.
- Guerrero, M., Satik, C., Finsterle, S., and Horne, R.N.: "Inferring Relative Permeability From Dynamic Boiling Experiments", Proceedings of 23rd Workshop on Geothermal Reservoir Engineering, Stanford University, Stanford, California (1998).
- Fourar, M., Bories, S., Lenormand, R., and Persoff, P.: Two-Phase Flow in Smooth and Rough Fractures: Measurement and Correlation by Porous-Medium and Pipe Flow Models, *Water Resources Research* **29** (11), (1993), pp 3699-3708.
- Honarpour, M., Koederitz, L.F., and Harvey, A.H.: Empirical Equations for Estimating Two-Phase Relative Permeability in Consolidated Rock, *JPT* (Dec. 1982), pp 2905-2909.
- Horne, R.N.: Notes on Geothermal Reservoir Engineering, Stanford University, Stanford, California (1991).

Horne, R.N., and Ramey, H.J., Jr.: Steam/Water Relative Permeability from Production Data, *GRC Trans.* **2** (1978).

Li, K., and Horne, R.N.: Accurate Measurement of Steam Flow Properties, *GRC Trans.* **23** (1999).

Mahiya, G.F.: *Experimental Measurement of Steam-Water Relative Permeability*, MS report, Stanford University, Stanford, CA (1999).

Mahiya, G., and Horne, R.N.: "Measurements of Steam-Water Relative Permeability", Stanford Geothermal Program Quarterly Report April-June 1998, Stanford University, Stanford, California.

Monsalve, A., Schechter, R.S., and Wade, W.H.: Relative Permeabilities of Surfactant/Steam/Water Systems, Paper SPE/DOE 12661, presented at the Society of Petroleum Engineers Symposium on Enhanced Oil Recovery, Tulsa, Oklahoma, April 1984.

Pan, X., Wong, R.C., and Maini, B.B.: Steady State Two-Phase Flow in a Smooth Parallel Fracture, presented at the 47th Annual Technical Meeting of The Petroleum Society in Calgary, Alberta, Canada, June 10-12, 1996.

Persoff, P., and Pruess, K.: Two-Phase Flow Visualization and Relative Permeability Measurement in Natural Rough-Walled Fractures, *Water Resources Research* **31** (5), (1995), pp 1175-1186.

Persoff, P., Pruess, K., and Myer, L.: Two-Phase Flow Visualization and Relative Permeability Measurement in Transparent Replicas of Rough-Walled Fractures, *Proceedings*, 16th Workshop on Geothermal Reservoir Engineering, Stanford University, Stanford, CA, Jan. 23-25, 1991, pp 203-210.

Piquemal, J.: Saturated Steam Relative Permeabilities of Unconsolidated Porous Media, *Transport in Porous Media* **17** (1994), pp 105-120.

Pruess, K., and Tsang, Y.W.: On Two-Phase Relative Permeability and Capillary Pressure of Rough-Walled Rock Fractures, *Water Resources Research* **26** (9), (1990), pp 1915-1926.

Rangel-German, E., Akin, S., and Castanier, L.M.: Multiphase Flow Properties of Fractured Porous Media, paper SPE 54591, presented at the SPE Western Regional Meeting, Anchorage, AK, May 26-28, 1999.

Romm, E.S.: *Fluid Flow in Fractured Rocks*, Nedra Publishing House, Moscow, (English translation, Blake, W.R., Bartlesville, OK, 1972).

Rossen, W.R., and Kumar, A.T.A.: Single- and Two-Phase Flow in Natural Fractures, paper SPE 24915, presented at the 67th Annual Technical Conference and Exhibition of the Society of Petroleum Engineers, Washington DC, Oct. 4-7, 1992.

Sanchez, J.M., and Schechter, R.S.: Comparison of Two-Phase Flow of Steam/Water through an Unconsolidated Permeable Medium, *SPE Reservoir Engineering*, Aug. (1990), pp 293-300.

Satik, C.: “Experiments of Boiling in Porous Media”, *Proceedings 22nd Workshop on Geothermal Reservoir Engineering*, Stanford University, Stanford, California (1997).

Satik, C.: A Measurement of Steam-Water Relative Permeability, *Proceedings 23rd Workshop on Geothermal Reservoir Engineering*, Stanford University, Stanford, CA (1998).

Satik, C., and Horne, R.N.: “Measurement of Steam-Water Relative Permeability,” Quarterly report for January – March 1998 Stanford Geothermal Program, DE-FG07-95ID13370.

Schembre, J.M., Akin, S., Castanier, L.M., and Kovscek, A.R.: “Spontaneous Water Imbibition into Diatomite,” paper SPE 46221, presented at the 1998 Western Region Meeting, Bakersfield, California, May 10-13.

Verma, A., and Pruess, K.: Enhancement of Steam Phase Relative Permeability Due to Phase Transformation Effects in Porous Media, *Proceedings 11th Workshop on Geothermal Reservoir Engineering*, Stanford University, Stanford, CA (1986).

Wang, C.T., and Horne, R.N.: Boiling Flow in a Horizontal Fracture, submitted to *Geothermics*, 1999.

Wel, K.K., Morrow, N.R., and Brower, K.R.: “Effect of Fluid, Confining Pressure, and Temperature on Absolute Permeabilities of Low-Permeability Sandstones,” *SPE Formation Evaluation* (August 1986), 413-423.